

Article

Study on Numerical Simulation Methods for Hypervelocity Impact on Large-Scale Complex Spacecraft Structures

Yanxi Zhang, Fengjiang An ^{*ID}, Shasha Liao, Cheng Wu, Jian Liu and Yipeng Li

State Key Laboratory of Explosion Science and Technology, Beijing Institute of Technology, Beijing 100081, China; 3120190270@bit.edu.cn (Y.Z.); haha121@bit.edu.cn (S.L.); chengwu@bit.edu.cn (C.W.); 3120195176@bit.edu.cn (J.L.); 3220200133@bit.edu.cn (Y.L.)

* Correspondence: anfengjiang@bit.edu.cn

Abstract: This paper aims to study the difference of results in breakup state judgment, debris cloud and fragment characteristic parameter during hypervelocity impact (HVI) on large-scale complex spacecraft structures by various numerical simulation methods. We compared the results of the test of aluminum projectile impact on an aluminum plate with the simulation results of the smooth particle hydrodynamics (SPH), finite element method (FEM)-smoothed particle Galerkin (SPG) fixed coupling method, node separation method, and finite element method-smooth particle hydrodynamics adaptive coupling method under varying mesh/particle sizes. Then based on the test of the complex simulated satellite under hypervelocity impact of space debris, the most applicable algorithm was selected and used to verify the accuracy of the calculation results. It was found that the finite element method-smooth particle hydrodynamics adaptive coupling method has lower mesh sensitivity in displaying the contour of the debris cloud and calculating its characteristic parameters, making it more suitable for the full-scale numerical simulation of hypervelocity impact. Moreover, this algorithm can simulate the macro breakup state of the full-scale model with complex structure and output debris fragments with clear boundaries and accurate shapes. This study provides numerical simulation method options for the follow-up research on breakup conditions, damage effects, debris clouds, and fragment characteristics of large-scale complex spacecraft.

Keywords: hypervelocity impact; numerical simulation; finite element method-smooth particle hydrodynamics adaptive coupling method; smooth particle hydrodynamics method; satellite damage



Citation: Zhang, Y.; An, F.; Liao, S.; Wu, C.; Liu, J.; Li, Y. Study on Numerical Simulation Methods for Hypervelocity Impact on Large-Scale Complex Spacecraft Structures. *Aerospace* **2022**, *9*, 12. <https://doi.org/10.3390/aerospace9010012>

Academic Editor: Pierre Rochus

Received: 17 November 2021

Accepted: 22 December 2021

Published: 25 December 2021

Publisher's Note: MDPI stays neutral with regard to jurisdictional claims in published maps and institutional affiliations.



Copyright: © 2021 by the authors. Licensee MDPI, Basel, Switzerland. This article is an open access article distributed under the terms and conditions of the Creative Commons Attribution (CC BY) license (<https://creativecommons.org/licenses/by/4.0/>).

1. Introduction

Space debris of any size poses a potential and actual threat to the operating spacecraft and the near-earth space ecology. In the low orbit area with the highest debris density, the relative velocity of the spacecraft and orbital debris could exceed 15 km/s. At such a velocity, impact with large as well as 1 cm or even smaller debris could cause serious or even catastrophic damage to the spacecraft [1]. Therefore, it is necessary to study the hypervelocity impact between space debris and large-scale complex spacecraft. Research on problems in hypervelocity impacts is quite different from those of high- and low-velocity impact. When the impact velocity exceeds 3 km/s, it is very difficult to perform the test and the required test conditions are more demanding, and it is also difficult to acquire debris information and images, especially for such problems as space debris impacting spacecrafts or ballistic missile interception at hypervelocity. Therefore, this study is to find appropriate numerical simulation means to present the problem of hypervelocity impact more accurately on full-scale complex structures, and then accurately simulate and analyze their breakup, characteristic parameters of debris cloud and debris fragments as well as the dynamic response of materials and structures under hypervelocity impact, and finally perform test verification. The selected appropriate simulation method can also be extended to the calculation of larger-scale hypervelocity impact problems, thus better-guiding follow-up tests, reducing research costs, and improving research efficiency.

However, the numerical simulation of hypervelocity impacts is essentially a highly nonlinear dynamic matter. The commonly used methods to solve such problems are the Lagrange method, Eulerian method, Arbitrary Lagrangian–Eulerian (ALE), and meshless method. In recent years, the smooth particle hydrodynamics (SPH) method as a meshless method has been developed rapidly and played a key role in hypervelocity impact studies. However, these methods all have their limitations. In the Lagrange method, the impactor and target are eroded after impact, and cannot form an effective debris cloud. In the Eulerian method, the accurate debris cloud cannot be formed after impact, and situation of the middle and rear parts of the impactor is obviously inconsistent with the test results [2]. The ALE method is suitable for the conditions that the initial impact objects are composed of solid and fluid, and that the material interface and the multiphase contact points are seriously deformed. This algorithm improves the calculation accuracy [3] but reduces the calculation efficiency compared with the Lagrange method and the Euler method. In addition, there exists a problem that the boundary is not well-defined for substances treated as liquids. In the numerical simulation of hypervelocity impact using the SPH method, the debris cloud formed is composed of discrete particles, so the boundary of the debris cloud is fuzzy, and it is difficult to determine the debris shape; moreover, it is hard to identify a single fragment and the interface between the cracked and uncracked material, and there is no recognized criterion yet, so it cannot accurately describe the shape and quantity of debris fragments. Furthermore, for the full-scale complex object under hypervelocity impact, the research involves the contact, boundary, connection, and failure setting among components, which also poses a new challenge to the selection of simulation algorithms.

To address the problem of debris fragment recognition, researchers have proposed many methods, such as linked lists, hierarchical tree methods, linked list-based search algorithm, and breadth-first search (BFS) [4–8], but they all determine the fragment based on the particle position at a specific time [9]. Therefore, there are limitations in terms of computational cost, the feasibility of applying algorithms in the calculation of full-scale complex models, and the accuracy and uniformity of fragment shape recognition.

In view of the inherent defects of the SPH method, many studies have made improvement to address its computational instability, debris fragment identification, and boundary problems, which have been successfully applied to hypervelocity impact research. Libersky et al. [10] improved the SPH method with tensile instability and without obvious boundary using the conservative smoothing method and FLIP code. Sakongaet et al. [11] proposed the criterion of using the k-means algorithm to determine the same fragment from similar trajectories, which improved the accuracy of fragment recognition. Zhang Xiaotian et al. [12,13] proposed the finite element reconstruction (FER) method, which uses the SPH method for solution, and then uses vector coordinate interpolation and deletes failure elements, thus realizing finite element reconstruction. Compared with the 200 mm satellite model with a simple structure, their effects are in good agreement. Compared with the SPH method, the FER method can give the debris fragment shape and other information, but its computational efficiency remains low and the material boundary is not clear. Moreover, existing research lacks the analysis of the comparison and verification of the test results against calculation results by the simulation algorithms in hypervelocity impact on the large-scale simulated complex spacecraft structure.

To solve the problem that a single meshless method fails to produce good calculation results, researchers have tried to couple the finite element method (FEM) and the meshless method, namely, conducting fixed coupling of the FEM and the calculation region of particles at the beginning of calculation time. It is found that this method can better simulate the perforation characteristics in hypervelocity impact problems [14,15], but problems such as complex modeling, difficulty in obtaining fragment information, and tensile instability still exist. Therefore, researchers began to study the adaptive coupling algorithm that automatically converts elements into particles in the calculation process. In 1994, Johnson [16] proposed the idea of transforming elements into particles using the element equivalent plastic failure criterion, and then improved and established the adaptive

coupling algorithm, but tensile instability remains a problem. Subsequently, many domestic and foreign researchers used different methods and failure criteria to study the adaptive coupling algorithm [17–20]. Compared with other literature, He et al. [21] improved the FEM-SPH adaptive coupling algorithm using the Johnson–Cook failure criterion and maximum tensile stress failure criterion, and the calculated results of characteristics and distribution of projectile spallation and debris cloud are in good agreement with the test results.

He et al.'s improved FEM-SPH adaptive coupling algorithm has advantages in dangerous debris fragment characteristic recognition and computational efficiency and also has good applicability in mesoscopic modeling. It may be an effective way of numerical simulation of hypervelocity impact on complex materials. However, for the dynamic response of different research object materials under high-velocity impact, the emerging smooth particle Galerkin (SPG) method [22] and the previous node separation algorithm [23,24] perform better than the FEM-SPH coupling method in many aspects, such as contact setting, the effect of coupling with the FEM, and sensitivity of failure criterion. The advantages and disadvantages of each algorithm are shown in Figure 1.

Many researchers have made valuable studies on the law of hypervelocity impact between space debris and spacecraft. Smirnov et al., used projectiles and shells of different materials (e.g., organic glass, aluminum, iron, and platinum) to carry out triple contact points hypervelocity impact numerical research on spherical thin-walled metal shell filled with ideal gas [3]. Liu et al., established two parameterized 2D numerical models using the SPH and the FEM studied the characteristics of the polyimide flow field and proposed a dynamic fracture strain criterion [25]. Rumyantsev et al., study the efficiency of screen protection of space vehicles against hypervelocity elongated projectiles that are an analog of the most dangerous space debris [26]. Shkirzyanova et al., conducted numerical simulations using the ANSYS Autodyn software package to study the behavior of transparent spacecraft components composed of multilayer glass plates (including transparent ceramics and polymers) impacted by different objects at high velocities (up to 1 km/s) and hypervelocity (up to 10 km/s) [27]. Toor et al., conducted two-dimensional, continuum shell, and three-dimensional modeling of a shielding system using the finite element method. The effect of thickness and velocity variation has been emphasized with a view to simulate the effect of space debris on the metallic shielding system [28]. In addition to the research on the hypervelocity impact of individual components on spacecraft, Schimmerohn et al., established a numerical tool PHILOS-SOPHIA and used the FEM-SPH coupling method to simulate the impact between the ESA LOFT satellite model and small satellites under different impact geometries. It was found that the fluid coding results showed good agreement and obvious deviation from the Standard Satellite Breakup Model (SSBM) prediction, and the simple energy-to-mass ratio (EMR) criterion failed to reflect such complexity [29]. Finally, concerning the comparison between the numerical simulation results and the experimental results, Meshkov et al., proposed a new algorithm to obtain the image edges by comparing the physical experiments and the calculation experiments based on fuzzy set theory and established an integrated system for modeling hypervelocity interaction of solids [30].

The main novelties are the establishment of the keywords and parameters of several numerical simulation algorithms in the field of hypervelocity impact, the study of the sensitivity of different algorithms to the mesh size, and the comparison of the accuracy of the algorithms based on the exact solution, experimental data, and the accumulated error. Based on this, this study provides a set of suitable parameters for simulating the hypervelocity impact of large-scale complex spacecraft, and studies the applicability to non-symmetric targets (different impact positions).

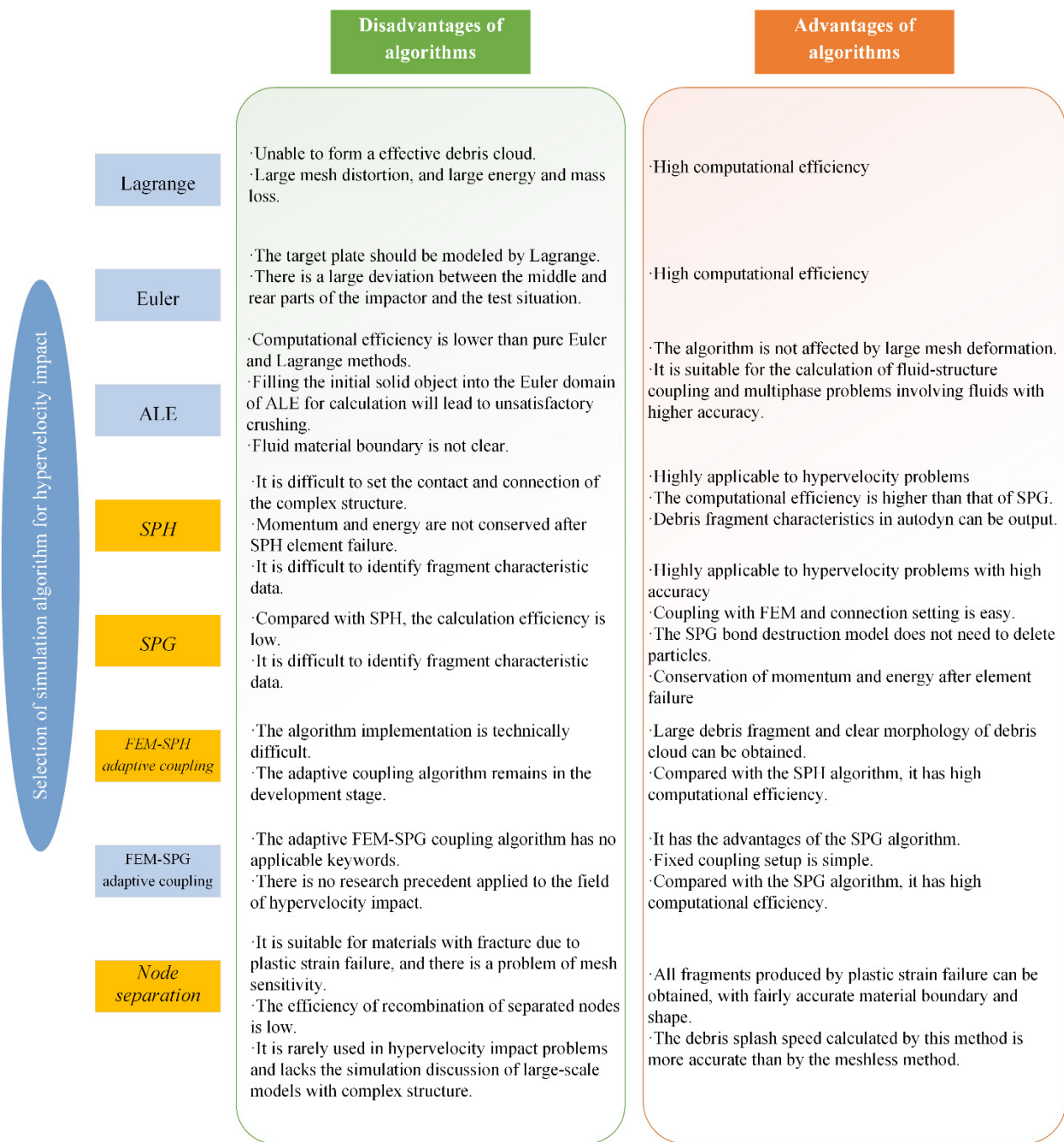


Figure 1. Advantages and disadvantages of algorithms for hypervelocity impact problems.

Among the four algorithms that may be applicable to the full-scale numerical simulation of hypervelocity impact, namely, the SPH method, FEM-SPH adaptive coupling method, FEM-SPG fixed coupling method, and node separation algorithm, the applicability of the FEM-SPG fixed coupling method and node separation algorithm in hypervelocity problems were rarely discussed, and few researchers have compared the test data of debris fragment characteristic parameters obtained by the SPH method and FEM-SPH adaptive coupling method to verify the accuracy of simulation and calculation in the full-scale model with complex structure. In addition, existing research lacks the comparative analysis of the applicability of the four algorithms for the same hypervelocity impact scenario, and for the problem of large-scale spacecraft under hypervelocity impact in the future, testing of the necessary algorithms' dependence on the mesh size is far from adequate.

Therefore, this paper will first compare the simulation results of SPH, FEM-SPG fixed coupling method, node separation method, and FEM-SPH adaptive coupling method under varying mesh/particle sizes with the test results of aluminum projectile impact on aluminum plate, so as to find the algorithm more suitable for the full-scale numerical simulation of hypervelocity impact that releases huge kinetic energy. Then, it is applied to the simulation and calculation of the hypervelocity impact of space debris on a simulated satellite. By comparing the debris' statistical simulation results with the test results, the applicability of the algorithm for hypervelocity impact simulation analysis of the full-scale complex spacecraft structure is verified. The main research content of this paper is shown in Figure 2.

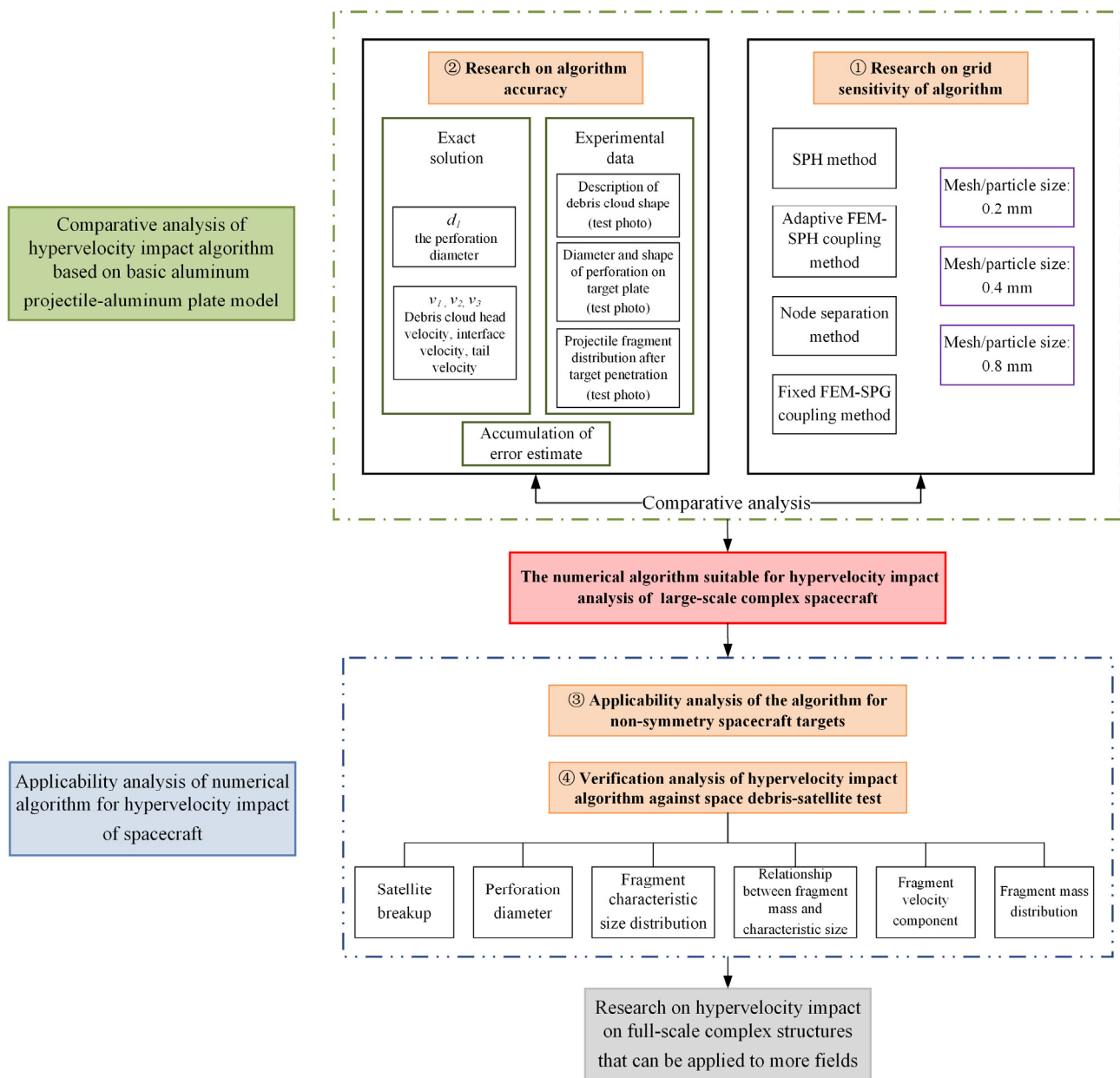


Figure 2. Logic diagram of the main research content.

2. Theory of Simulation Algorithms

2.1. Smooth Particle Hydrodynamics Method

The smooth particle hydrodynamics (SPH) method is a pure Lagrangian particle method developed in the past three decades. It can deal with many large deformation

problems without meshes but retains the advantages of the Lagrangian method. In 1993, Libersky et al. [31] applied the SPH method to elastoplastic solid dynamics problems for the first time and proposed the three-dimensional impact and material response code based on smooth particle hydrodynamics.

The core of this method is an interpolation technique. Particle A will interact with other particles within two times the smoothing length. All macro variables can be calculated by expressing the values on a set of disordered points as integral interpolation in the form of:

$$\langle f(x) \rangle = \int_{\Omega} f(x') W(x - x', h) dx' \quad (1)$$

where Ω —the whole solution region, $W(x - x', h)$ —the kernel function, h —the SPH particle smoothing length, which is used to define the influence of a particle on the surrounding region.

Considering spatial discretization, Equation (1) is approximately transformed into summing each particle in the calculation domain Ω :

$$\langle f(x) \rangle = \int_a f(x') W(x - x', h) dx' = \sum_{j=1}^N f(x_j) W(x - x_j, h) \Delta V_j \quad (2)$$

where ΔV_j represents the volume of particle j . If the particle density is defined as ρ_j , the particle mass can be expressed as:

$$m_j = \Delta V_j \rho_j \quad (3)$$

Substituting Equation (3) into Equation (2), we obtain:

$$\langle f(x) \rangle = \sum_{j=1}^N \frac{m_j}{\rho_j} f(x_j) W(x - x_j, h) \quad (4)$$

Therefore, the approximate formula of the function at particle i can be expressed as:

$$\langle f(x) \rangle = \sum_{j=1}^N \frac{m_j}{\rho_j} f(x_j) W_{ij} \quad (5)$$

where $W_{ij} = W(x - x_j, h)$.

As can be seen from Equation (5), any function value at particle i can be obtained by applying the kernel function to the weighted average of the functions corresponding to all particles in its calculation domain. If the density function ρ is used in Equation (5) instead of the function $f(x)$, then the SPH approximate formula of density is:

$$\rho_i = \sum_{j=1}^N m_j W_{ij} \quad (6)$$

Similarly, the function derivative at particle i in the SPH method is expressed as:

$$\langle \nabla \cdot f(x_i) \rangle = \sum_{j=1}^N \frac{m_j}{\rho_j} f(x_j) \cdot \nabla W_{ij} \quad (7)$$

To sum up, the core conservation equations used in the SPH method are:

The law of mass conservation:

$$\frac{d\rho_i}{dt} = \rho_i \sum_{j=1}^N \frac{m_j}{\rho_i} (u_i - u_j) \nabla W_{ij} \quad (8)$$

The law of momentum conservation:

$$\frac{du_i}{dt} = -\sum_{j=1}^N m_j \left(\frac{p_j}{\rho_i^2} + \frac{p_j}{\rho_j^2} \right) \nabla W_{ij} \quad (9)$$

The law of energy conservation:

$$\frac{dE_i}{dt} = \frac{p_j}{\rho_i^2} \sum_{j=1}^N m_j (u_i - u_j) \nabla W_{ij} \quad (10)$$

2.2. Smoothed Particle Galerkin Method

When used in hypervelocity impact problems, the traditional FEM often requires element deletion and other failure analysis, and then mass and energy are not conserved. When the deviation is too large, it will have a great impact on the accuracy of the simulation results. However, the traditional SPH meshless method has such problems as being unable to ensure convergence, tensile instability caused by kernel functions, etc. Therefore, in order to obtain a more stable and accurate numerical solution from the original point integration meshfree Galerkin method, Livermore Software Technology Corporation (LSTC) developed the SPG method, and derived the numerical stability enhancement term by smoothing the displacement, thus obtaining a more stable numerical solution [32]. The SPG method mainly uses the bond failure between particles to generate fracture, which has been successfully applied to metal cutting, high-velocity impact, penetration, and other fields.

In general, when explicit dynamics is used to solve problems, the semi-discrete equation is solved as follows:

$$M^{lump} \ddot{U} = f^{ext} - f^{int} \quad (11)$$

where M^{lump} —the concentrated mass, f^{ext} —the external force, f^{int} —the internal force. When the direct point integration is used for solution, the low-energy mode will appear.

Therefore, LSTC establishes the SPG algorithm, where smooth strain is added to smooth the displacement, and the stability enhancement term is derived. Thus, Equation (11) can be derived into the following form:

$$M^{lump} \ddot{U} = f^{ext} - f^{int} - f^{stb} \quad (12)$$

where f^{stb} —the stability enhancement term derived for smooth displacement from SPG. The expression of f^{stb} is obtained by direct point integration:

$$f^{stb}_I \stackrel{DNI}{=} \sum_{N=1}^{NP} B_I^T(X_N) P(X_N) V_N^0 = \sum_{N=1}^{NP} B_I^T(X) \sigma(X_N) J^0 V_N^0 \quad (13)$$

where B is the gradient matrix related to the displacement smoothing function and displacement approximation function, and σ is the stability enhancement stress [33].

2.3. Finite Element Method-Smooth Particle Hydrodynamics Adaptive Coupling

The keyword DEFINE_ADAPTIVE_SOLID_TO_SPH in LS-DYNA can be used to realize the FEM-SPH adaptive coupling method. It is also required to define in the K file the solid part ID that needs particle conversion, the number of SPH particles generated by each mesh, the coupling type between particles and other meshes as well as particle attributes. During simulation and calculation, using this keyword, the program will generate SPH particles with the same parameters on the geometric center of the corresponding mesh before calculation. The generated particles are constrained on the mesh and move with it. When the mesh reaches the failure conditions set for the material, the mesh is deleted and converted into the SPH particle that inherits the material properties and volume at the time of mesh failure according to the setting. Then the particle is set according to the keyword of

the K file and coupled with the remaining finite element meshes for subsequent calculation. The specific process is shown in Figure 3.

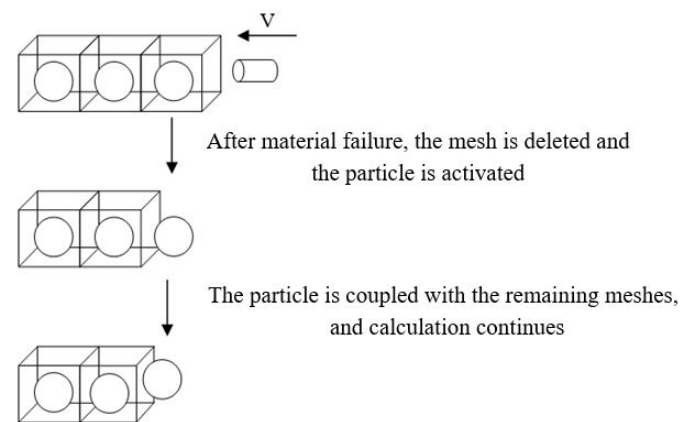


Figure 3. Process of finite element method-smooth particle hydrodynamics adaptive coupling method.

2.4. Node Separation Method

The node separation method is an improved version of the traditional Lagrange FEM. Between the traditional finite element meshes are conodes, and after conode separation, the conode is copied into different nodes with the same spatial position which are assigned to each separated mesh. In the node separation algorithm, a program is used to form a node set comprising nodes that belong to different meshes originated from the conode, and constraints are imposed on the node set. The nodes in the node set have the same degree of freedom in spatial motion. When the fracture criterion is met, the constraint is released, and then the nodes in the set will not transfer pressure to each other. The node separation algorithm separates the meshes through such a process and causes cracks without deleting certain meshes. The specific process is shown in Figure 4.

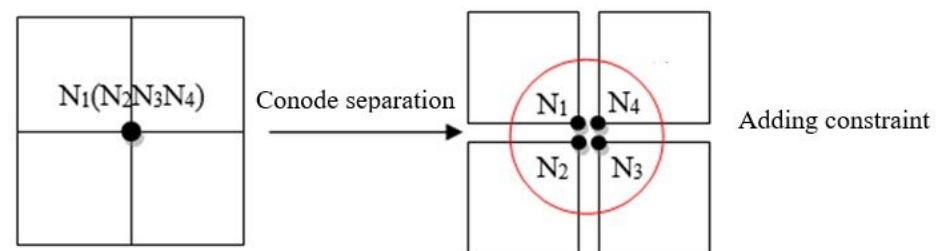


Figure 4. Process of node separation method.

3. Equations and Parameters of Simulated Materials

In the preliminary numerical simulation of hypervelocity impact, the material models used are as follows. The material state model adopts the Mie–Grüneisen equation of state (EoS) and shock EoS. The material strength models include the Johnson–Cook (JC) strength model and the Steinberg strength model, with the former mainly used in this study. For the material failure model, the Grady–Spall failure model is employed when using SPH for numerical simulation; instead, the JC failure model and maximum tensile stress failure criterion are employed for finite element mesh failure determination when using the FEM-SPH adaptive coupling method for simulation.

3.1. Equation of State of Materials

At present, the Mie–Grüneisen EoS and Tillosten EoS are mainly used in the numerical simulation of hypervelocity impacts, and this study mainly employs the Mie–Grüneisen

EoS. Two forms of Mie–Grüneisen EoS are defined in LS-DYNA and Autodyn, namely, Mie–Grüneisen EoS and Shock EoS, corresponding to the two different states of compression and expansion.

For materials under the state of compression, the hydrostatic pressure p is calculated by:

$$p = \frac{\rho_0 C^2 \mu \left(1 - \frac{\gamma_0}{2}\right) \mu - \frac{a}{2} \mu^2}{\left[1 - (S_1 - 1)\mu - S_2 \frac{\mu^2}{(\mu+1)^2} - S_3 \frac{\mu^3}{(\mu+1)^3}\right]^2} + (\gamma_0 + a\mu)E \quad (14)$$

For materials under the state of expansion, the following form is adopted:

$$p = \rho_0 C^2 \mu + (\gamma_0 + a\mu)E \quad (15)$$

In the above equations, ρ_0 is the initial density of the material, C is the sound velocity through the material, γ_0 is the Grüneisen coefficient, μ is the compression ratio, a is a first-order correction coefficient of γ_0 , S_1 , S_2 and S_3 are determined by the slope of the polynomial curve fitted between V_B and V_E sections in the curves of shock wave velocity U and particle velocity u_p . The Grüneisen EoS is more suitable to describe metals in a condensed state. It can describe the thermodynamic behavior of most metal solids in a condensed state but is not fit for liquid and gas phase regions.

3.2. Material Strength Model

In the numerical simulation of hypervelocity impacts, the commonly used material strength models are the Johnson–Cook strength model and Steinberg strength model. The former is selected because it considers the plastic strain rate and thermal softening, including phase transformation because melting and evaporation will occur during hypervelocity impact.

The Johnson–Cook strength model is an ideal rigid plastic strength model that can better reflect the strain rate strengthening effect and thermal softening effect of materials. In other words, the model mainly considers the influence of temperature and strain rate on the yield stress of materials and ignores the influence of external pressure.

In the JC model, the yield stress σ_y is expressed as:

$$\sigma_y = \left(A + B\varepsilon_p^n\right) \left(1 + C \ln \dot{\varepsilon}^*\right) \left(1 - T^{*m}\right) \quad (16)$$

where: ε —equivalent plastic strain, $\dot{\varepsilon}^* = \dot{\varepsilon}/\dot{\varepsilon}_0$ —the dimensionless equivalent plastic strain rate ($\dot{\varepsilon}_0$ is generally 1.0/s), A —the yield strength of the quasi-static material, B and n —the influencing factors of strain hardening, C —the strain rate sensitivity coefficient, m —the thermal softening index, the relative temperature $T^* = (T - T_t)/(T_m - T_t)$, where T_t is the room temperature and T_m the melting temperature. In Equation (16), the expression in the first bracket gives the strain strengthening effect; the second and third bracket terms represent the effects of strain rate and temperature on the yield stress of the material.

3.3. Material Parameters of Test of Aluminum Projectile Impact on Aluminum Plate and Test of Space Debris Impact on Simulated Satellite

This study uses Piekutowski's test of aluminum projectile impact on the aluminum plate [34,35] and Liu Sen's test of space debris impact on simulated satellite [36] for simulation comparison. In Piekutowski's test, the projectile material is a 2017-T4 aluminum alloy, and the plate material is a 6061-T6 aluminum alloy. As the 2017-T4 material parameters are difficult to determine, the 2024-T3 material parameters are adopted, and their performance is similar. According to Liu Sen's test, the projectile material simulating space debris is a 6061 aluminum alloy, the satellite plate material is a 2024 aluminum alloy, and the satellite electronic box material is a 6063 aluminum alloy. For impact at hypervelocity of 3.26 km/s, the selected material model needs to be adapted to the high strain rate ($>10^5$). Therefore, the JC strength model and the Mie–Grüneisen EoS are selected, and when using

the SPH for numerical simulation, the material failure model used is the Grady–Spall failure model (failure coefficient 0.15); when using the FEM-SPH adaptive coupling method for simulation, the JC failure model and the maximum tensile stress failure criterion are employed to simulate tensile failure and compression failure. After the finite element fails, the activated particle is set to $D1 = 1 \times 10^{-12}$ to make it ineffective once activated. In the SPG and node separation algorithms, the ultimate strain of 2024 aluminum alloy is set to $Fs = 0.186$ [37], and the ultimate strain of 2024 aluminum alloy $Fs = 0.88$ [38]. The material model parameters are shown in Table 1.

Table 1. Material parameters of simulation models [21,39].

Parameters	Symbol	2024 Aluminum Alloy	6063 Aluminum Alloy	6061 Aluminum Alloy
JC Model Parameters				
Density/($\text{kg}\cdot\text{m}^{-3}$)	R0	2780	2700	2700
Poisson's ratio	PR	0.33	0.33	0.33
Shear modulus/(GPa)	E	27.6	26.69	27.6
Static yield limit/(MPa)	A	265	200	290
Strain hardening modulus/(MPa)	B	426	144	203
Strain hardening exponent	n	0.34	0.62	0.35
Strain rate coefficient	C	0.015	0	0.011
Spall type	SPALL	3	3	3
Failure parameter D1	D1	0.8	0.2	1
Failure parameter D2-5	D2-5	0	0	0
Mie–Grüneisen/Shock EoS Parameters				
Sound velocity/($\text{m}\cdot\text{s}^{-1}$)	C	5386	5386	5386
Constant S_1	S_1	1.339	1.339	1.339
Constant γ	GMAO	1.97	1.97	1.97

4. Comparison of Simulation Algorithms Based on Test of Aluminum Projectile Impact on Aluminum Plate

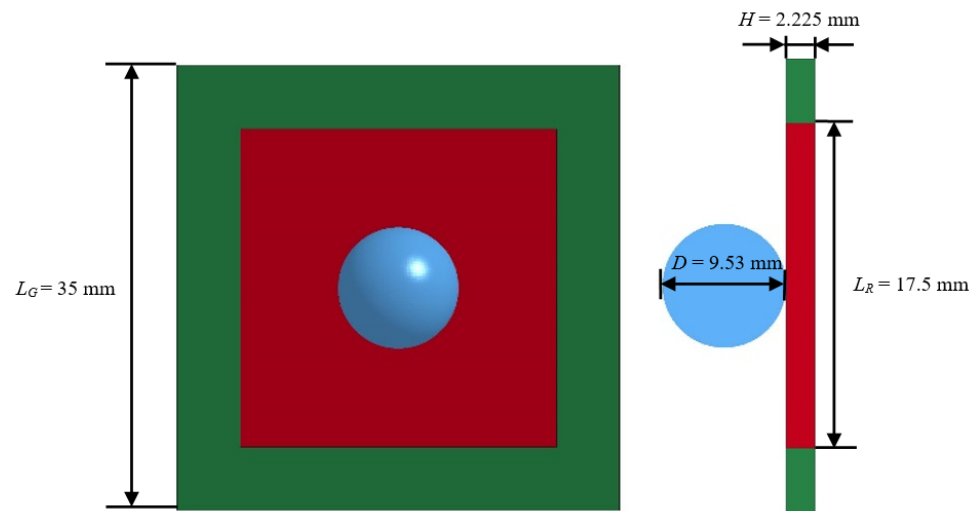
Hypervelocity impact is different from high-velocity impact in that the basic impact theory, breakup model, breakup conditions, material equation, and numerical simulation algorithm of the object under hypervelocity impact vary accordingly. Firstly, according to the calculation example of hypervelocity impact of the aluminum projectile which has been supported by tests [34,35], this study compares the four algorithms that may be suitable for numerical calculation of hypervelocity impact problems, studies the mesh sensitivity of each algorithm, and analyzes the hypervelocity impact simulation algorithm that is more suitable for the full-scale model with complex structure.

4.1. Establishment of Simulation Model

Based on Piekutowski's test [34,35], four numerical methods are established to reconstruct the test results. In the test, a two-stage light air gun is used to shoot aluminum projectiles and impact the aluminum plate. The test parameters are presented in Table 2. According to the test data in the table, a three-dimensional finite element model is established, as shown in Figure 5. In the figure, the projectile (the blue part) and the flat plate (the green and red parts) are divided into hexahedral Lagrangian elements at the initial moment.

Table 2. Control test parameters.

No.	Projectile Diameter (mm)	Projectile Material	Target Plate Thickness (mm)	Target Plate Material	Impact Velocity ($\text{km}\cdot\text{s}^{-1}$)
4-1352	9.53	2017-T4	2.225	6061-T6	6.64

**Figure 5.** (4-1352 test) simulation and calculation model.

In the full SPH algorithm, the entire model is converted into SPH particles of different sizes. In the FEM-SPH adaptive coupling algorithm, the keyword `DEFINE_ADAPTIVE_SOLID_TO_SPH` is used to delete the meshes in the blue and red parts due to failure during calculation and converted into particles, and since the meshes in the green part are too far away from the impact area, the above keyword is not set here to reduce the calculation time. In the FEM-SPG fixed coupling algorithm, the SPG algorithm is adopted for the blue and red parts in the main impact area, and the FEM is used for the green part for the sake of computational efficiency. In the node separation algorithm, node separation is performed by LS-PrePost in the impact area, and node constraints are added by self-programming. In the model, the distance between the projectile and the target plate is 0, the initial velocity of the projectile is shown in Table 2, under the condition of fixed periphery of the plate.

Regarding the settings of the four different simulation algorithms, first, the particle size is set to 0.1, 0.2, 0.4, and 0.8 mm [21] based on the SPH algorithm of ANSYS/Autodyn, the software's default SPH contact is used, and the safety factor is set to 0.667. The other three algorithms are realized with the keyword in the K file in ANSYS/LS-DYNA (units: m, kg, s).

Second, in the FEM-SPH adaptive coupling algorithm, the mesh sizes are set to 0.2, 0.4, and 0.8 mm [21]. To realize the algorithm function, the keyword `DEFINE_ADAPTIVE_SOLID_TO_SPH` is used to realize the adaptive FEM-SPH method, and the key parameter `ICPL = 1` and `IOPT = 1` are entered so that the SPH particles are constrained on the meshes in an inactive state before the corresponding meshes are deleted. After these meshes fail, the particles will be released, activated, and can be coupled with other particles and remaining elements. During calculation, the contact setting between the aluminum projectile and the aluminum plate is also critical, including the contact between the mesh surfaces of the projectile and the plate, the contact between internal meshes, and the contact between SPH particles and the remaining mesh elements. The keyword `CONTACT_ERODING_SURFACE_TO_SURFACE` is used to define the surface-to-surface contact erosion relationship between different solid elements. In this keyword, the components of aluminum projectile and aluminum plate are defined as the master segment

and the slave segment, and the static friction coefficient is set to $f_s = 1.05$ and the dynamic friction coefficient $f_d = 1.40$ for aluminum alloy materials. For single-node particles, the keyword `CONTACT_EROSION_NODES_TO_SURFACE` uses node-to-surface contact erosion conditions to define the contact relationship between particles and mesh elements. In this keyword, the particle is defined as the slave segment, and the remaining mesh elements are defined as the master segment. Here, when setting the contact between the particle and the mesh, one needs to set the parameter $ITHK = 1$ through the keyword `CONTROL_SPH`, so that the volume of an SPH particle is considered during contact. Besides surface contact, the spalling inside the projectile and the plate will make them contact each other in the same entity, which cannot be handled by the above two types of contact erosion methods. Therefore, it is necessary to set an additional keyword `CONTACT_INTERIOR` for the set of all solid elements to calculate the contact between the elements within the entity. At the same time, the control keyword `CONTROL_CONTACT` is added and the parameter `SLSFAC` is set to 10 to prevent the mutual penetration of the meshes. Finally, regarding the hourglass control parameters, for the SPH particles, in the keyword `CONTROL_SPH`, the parameter $IAVIS = 0$ is set in the Monaghan format. The hourglass coefficient `QM` in the keyword `HOURGLASS` does not have a specific selection theorem. As an empirical parameter, the user needs to set it within a certain range. In the calculation of the debris cloud problem, due to the high impact velocity, mutual penetration is likely to occur, so it is necessary to set the `QM` of the SPH particles and finite element to 1 to avoid such anomalies [21]. In addition, the hourglass control parameters also need to be considered. According to the results of the trial calculation, in the keyword hourglass corresponding to the keywords of the FEM and SPH, the parameter `IHQ` is set to 3, i.e., the Flanagan-Belytschko viscosity form is used for accurate volume integration. And for the FEM element, the parameters $Q1 = 1.5$ and $Q2 = 0.06$ are set in the keyword `HOURGLASS`.

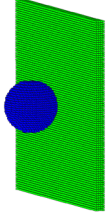
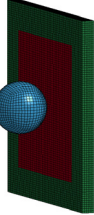

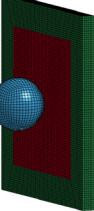
Third, in the FEM-SPG fixed coupling algorithm, the mesh and SPG particle size is set to 0.2, 0.4, and 0.8 mm [21]. To realize the algorithm function, Type 47 is selected in `ELFORM` of the keyword `SECTION_SOLID_SPG` to realize the SPG Method, where for the hypervelocity problem, the parameters $DX = DY = DZ = 1.5$ and $KERNEL = 2$ are set. Then, in Optional Card 3 of `SECTION_SOLID_SPG`, the damage mechanism options $IDAM = 1$, $ITB = 2$, and $ISC = 1$ and the effective plastic strain `FS` corresponding to the material are entered. Regarding the contact setting of the FEM-SPG fixed coupling algorithm, the keyword `CONTACT_TIED_SURFACE_TO_SURFACE` is used for the initial binding contact setting for the SPG impact area and the FEM non-impact area, and for the aluminum projectile and the aluminum plate in the impact area, `CONTACT_ERODING_NODES_TO_SURFACE` and `CONTACT_ERODING_SURFACE_TO_SURFACE` are used to define the contact relationship between two SPG PART, where the aluminum projectile is the slave surface and the aluminum plate the master surface. In addition, for the contact setting between the SPG area and the FEM area, the keyword `COTACT_AUTOMATIC_NODES_TO_SURFACE` is mainly employed to establish the contact relationship, where the SPG particle is the slave surface and the FEM surface the master surface, and the keyword `SOFT = 1` set in Optional Card A. Finally, similar to the adaptive FEM-SPH algorithm, it is also necessary to set an additional keyword `CONTACT_INTERIOR` for the set of all solid elements to calculate the contact between the elements within the entity. Meanwhile, the control keyword `CONTROL_CONTACT` is added and the parameter `SLSFAC` is set to 10 to prevent the mutual penetration of the meshes, and the calculated safety factor is set to 0.1.

Third, in the node separation algorithm, due to the limitation of the number of meshes on the running time of the node group program, the mesh sizes are set to 0.4 and 0.8 mm [21] at the beginning. To realize the algorithm function, the Detach function in Hyper Mesh is used to realize the separation of the impact area meshes. Then the self-made program is used to write the separated nodes at the same position into the node group `SET_NODE_LIST`. Afterwards, the keyword `CONSTRAINED_TIED_NODES_FAILURE` is used and $ETYPE=1$ is set so that the corresponding `EPPF` value can be input to impose

the effective plastic strain constraint on the node group. The contact setting of the node separation algorithm is basically the same as that of the fixed FEM-SPG constraint.

According to the test of aluminum projectile impact on aluminum plate, the simulation conditions of various mesh sizes under the four algorithms are studied and set, as shown in Table 3.

Table 3. Simulation conditions.

Algorithm	Mesh and Particle Size/(mm)	Schematic (Take 0.4 mm for Example)
SPH	0.1	
	0.2	
	0.4	
	0.8	
FEM-SPH adaptive coupling	0.2	
	0.4	
	0.8	
FEM-SPG fixed coupling	0.2	
	0.4	
	0.8	
Node separation	0.4	
	0.8	

4.2. Mesh Sensitivity Analysis for Different Algorithms

When the research object of hypervelocity impact problems expands to a large-scale object with a complex structure, the sensitivity of different algorithms to mesh size becomes a factor affecting the selection of algorithms. Due to the limitation of existing computing resources and software's computational capacity, for the same full-scale computation model, on the basis of meeting the mesh accuracy required for the analysis of debris fragment shape after impact, the smaller the impact of mesh size setting on the calculation results, the smaller the order of magnitude of meshes involved in the calculation, so that the calculation can be carried out or the computational efficiency can be improved. Therefore, the study is designed according to the simulation conditions, and the influence of mesh accuracy on the calculation results under the four algorithms is compared with the simple aluminum projectile-aluminum plate model.

4.2.1. Smooth Particle Hydrodynamics Algorithm

In the SPH algorithm, the particle sizes are set to 0.1, 0.2, 0.4, and 0.8 mm. First, to analyze the influence of mesh size on the calculation results of the debris cloud, the

characteristic parameters of debris cloud at $6 \mu\text{s}$ after impact under the four mesh sizes are studied and compared [35], including α —debris cloud reverse splash angle, β —debris cloud diffusion angle, d_1 —the perforation diameter, d_2 —the maximum diameter of the debris cloud, h —distance from the front end of the debris cloud to the target plate, v_1 —velocity in the high-velocity stage of the debris cloud, v_2 —velocity in the medium-velocity stage of the debris cloud, v_3 —velocity in the low-velocity stage of the debris cloud. The geometric significance of each parameter is shown in Figure 6.

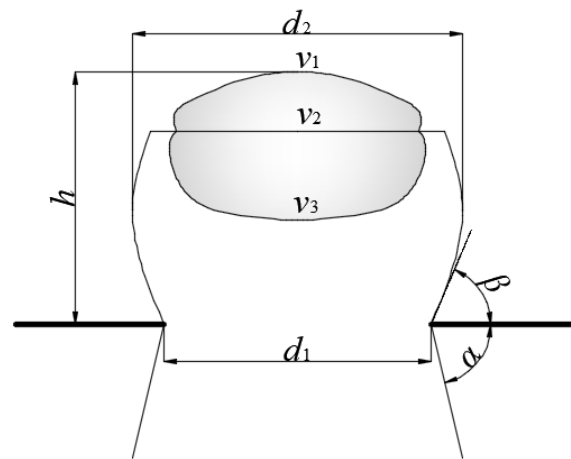


Figure 6. Characteristic parameters of debris cloud.

After the calculation of simulation conditions of the four particle sizes is completed, the contour graphs of the debris clouds at $6 \mu\text{s}$ are shown in Figure 7. It can be roughly seen from these contours and section graphs that although the SPH method has the problem of the unclear boundary of the debris cloud and fragments, as the particles become finer, the contour of the debris cloud becomes clearer; on the contrary, the larger the particles, the less clear the contour of the debris cloud, and the more difficult and less accurate the statistics of characteristic parameters. At the same time, as illustrated, the smaller the particle size, the larger the diffusion angle, and the other data need to be measured accurately.

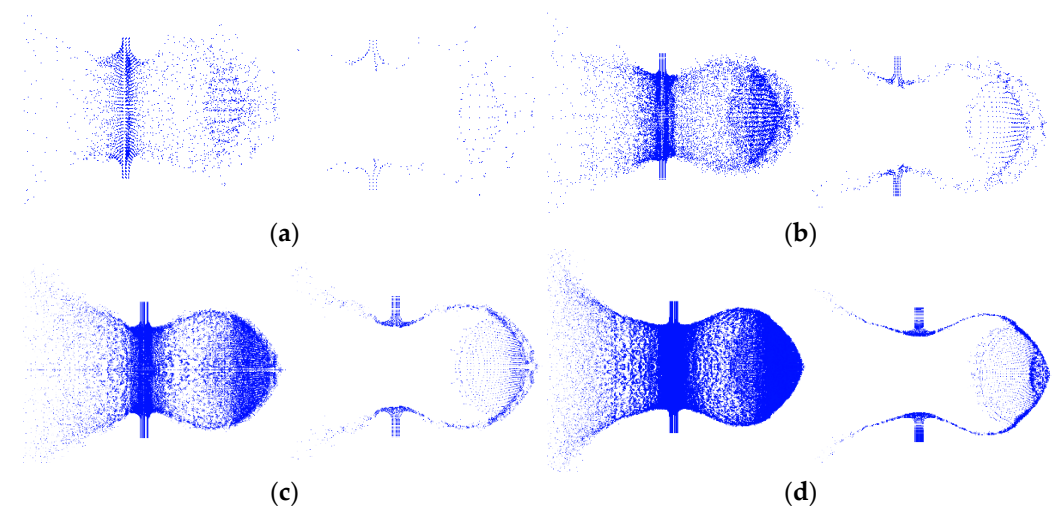


Figure 7. Contours and section graphs of debris cloud under different particle sizes. (a) Particle size 0.8 mm; (b) particle size 0.4 mm; (c) particle size 0.2 mm; (d) particle size 0.1 mm.

Furthermore, to compare the stability of the calculation results of the debris cloud characteristic parameters under different particle sizes, the measurement function of Autodyn and tools such as GetData are used to measure the characteristic parameter values under

the simulation conditions. The changes in each value are shown in Figure 8. Observing the changes in the curves, we can find that for the perforation diameter d_1 and the maximum diameter of the debris cloud d_2 , the perforation diameter has a large increase ($>7\%$) when the particle size is 0.8 mm, and in other situations, the basic changes are not large with the fluctuation not exceeding 1.28 mm ($<5\%$). However, the distance h from the front end of the debris cloud to the target plate is greatly affected by the particle size. As the particle size increases, h also gradually increases, with a change of 3.68 mm ($>10\%$). At the same time, the ricochet and diffusion angles basically decrease as the particles become coarser, and the change is obviously greater than 15%. The ricochet angle changes more drastically ($>25\%$) than the diffusion angle. Therefore, in the SPH method, the particle size has a great impact on the overall contour of the debris cloud. Finally, regarding the three-stage velocity of the debris cloud, the velocity in the high-velocity and low-velocity stages decreases with the refinement of the particles. On the contrary, the velocity in the medium-velocity stage increases, and the particle size has a greater impact on the head and tail velocities. The velocity deviation in the high-velocity stage is $620.7 \text{ m}\cdot\text{s}^{-1}$, and that in the low-velocity stage is $1212.4 \text{ m}\cdot\text{s}^{-1}$.

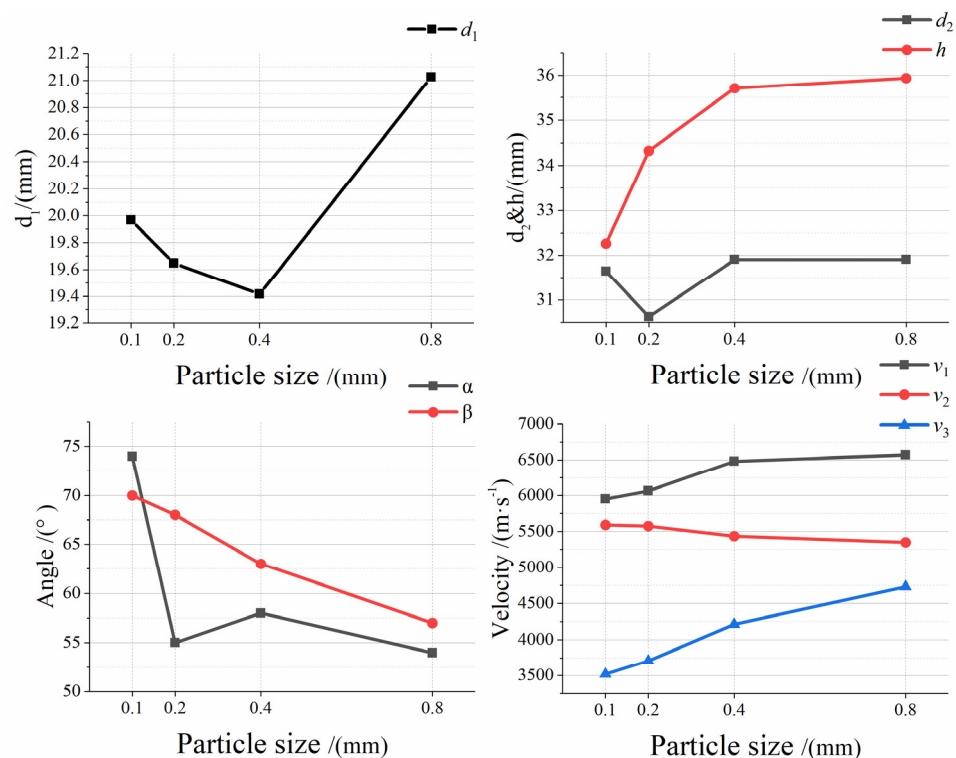


Figure 8. Curves of characteristic parameter values under different particle sizes.

In summary, the particle size has little effect on the perforation diameter d_1 of the debris cloud, the maximum diameter d_2 of the debris cloud, and the velocity v_2 in the debris cloud's medium-velocity stage, but its effect on the distance h from the front end of the debris cloud to the target plate, ricochet angle, diffusion angle as well as velocity in the low- and high-velocity stages is significant.

In addition to analyzing the characteristics of the debris cloud, the debris fragment information is also very important. To analyze the influence of mesh size on the calculation results of debris fragment characteristics, the characteristic parameters of the remaining fragments of the aluminum projectile and aluminum plate at $6 \mu\text{s}$ after impact is studied and compared, including fragment location distribution, fragment characteristic length (L_c) distribution, fragment mass (m) distribution and the relationship between mass and characteristic length. Regarding the debris fragment distribution, according to the data output by Autodyn, the number of effective fragments calculated under the particle size of 0.1, 0.2,

0.4, and 0.8 mm is 2803, 1688, 200, and 2, respectively. Therefore, the finer the particles, the more effective the fragments obtained. However, as the SPH method does not display clear boundaries of fragments, and the fragment data output by American ANSYS Autodyn cannot distinguish between metal particles in the debris clouds and visible fragments, fragments can be reconstructed but it is difficult to analyze their approximate distribution. The fragment characteristic length distribution, mass distribution, and relationship between mass and characteristic length can be statistically obtained by inputting the data output by Autodyn into Origin. Considering that Autodyn only outputs one effective fragment of data under the particle size of 0.8 mm, it is not included in the statistics.

Firstly, the characteristic length distribution of debris fragments in the logarithmic coordinate system of different particle sizes is shown in Figure 9a. From the trend of the curves, when the particle size is expanded to 0.4 mm, the distribution curve is far away from those of the finer particles. The two distribution curves for particle sizes of 0.2 and 0.1 mm are close and similar, and the cumulative number of fragments with a characteristic length of over 1 mm has a linear relationship with a characteristic length. Therefore, it is best to build particles with $1/5\sim 1/10$ of the characteristic size of debris fragments to be studied using the SPH method, and the straight line fitted by the two distribution curves for particle sizes of 0.2 and 0.1 mm when the characteristic length is greater than 1 mm is shown in Figure 9b.

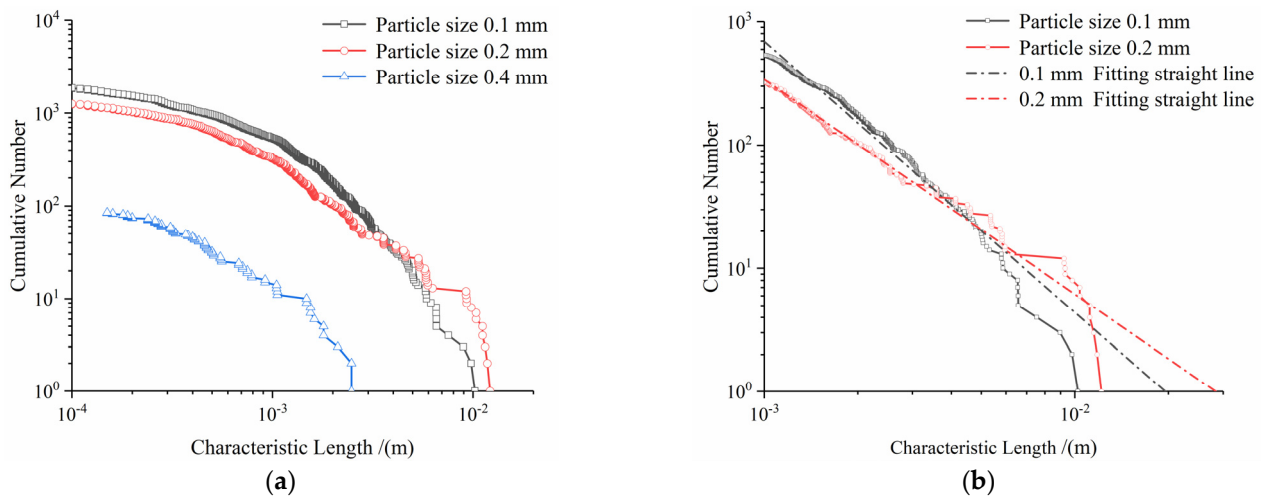


Figure 9. Characteristic length distribution of debris fragments under different particle sizes. (a) Characteristic length distribution of debris fragments under three particle sizes; (b) characteristic length ($>10^{-3}$ m) distribution of debris fragments in the case of fine particles.

Secondly, the mass distribution of debris fragments in the logarithmic coordinate system of different particle sizes is shown in Figure 10a. From the trend of the curves, compared to the characteristic length, the particle size has a greater impact on the statistics of fragments with small masses but has a smaller impact on the slope. Furthermore, for masses greater than 10^{-7} kg, the mass distribution curve shows a linear relationship. The straight line fitted by the two distribution curves for particle sizes of 0.2 and 0.1 mm when the mass is greater than 10^{-7} kg is shown in Figure 10b. As illustrated, the two curves for particle sizes of 0.2 and 0.1 mm almost coincide in the range of $10^{-7}\sim 10^{-6}$ but differ greatly in the case of larger masses.

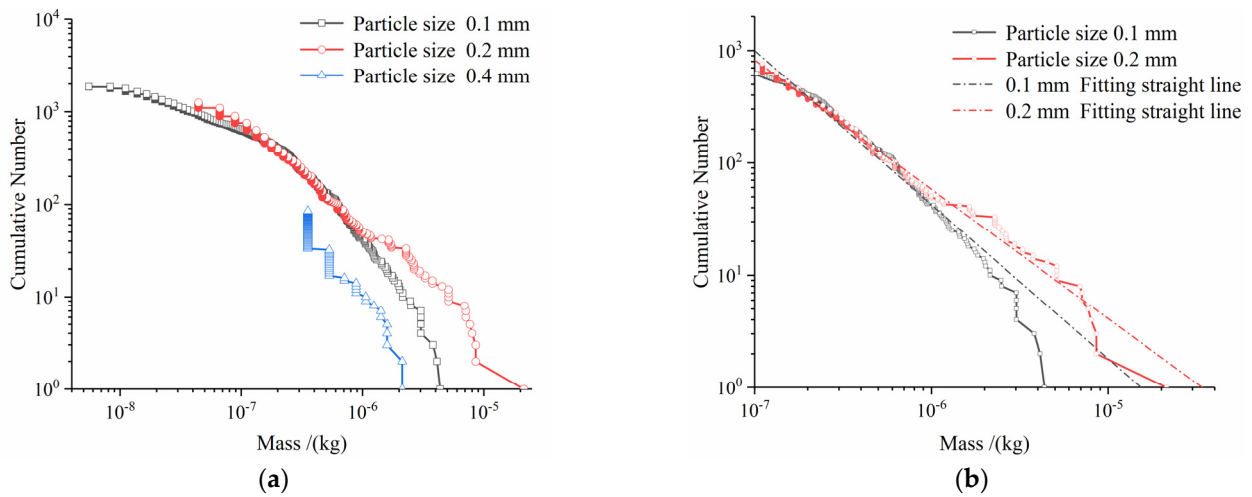


Figure 10. Mass distribution of debris fragments under different particle sizes. (a) Mass distribution of debris fragments under three particle sizes; (b) mass (>10⁻⁷ kg) distribution of debris fragments in the case of finer particles.

Finally, the characteristic length–mass relationship of fragments in the logarithmic coordinate system of different particle sizes is presented in Figure 11. According to the figure, their relationship is greatly affected by the particle size when the characteristic length is in a small order of magnitude, and this influence becomes smaller as the characteristic length increases.

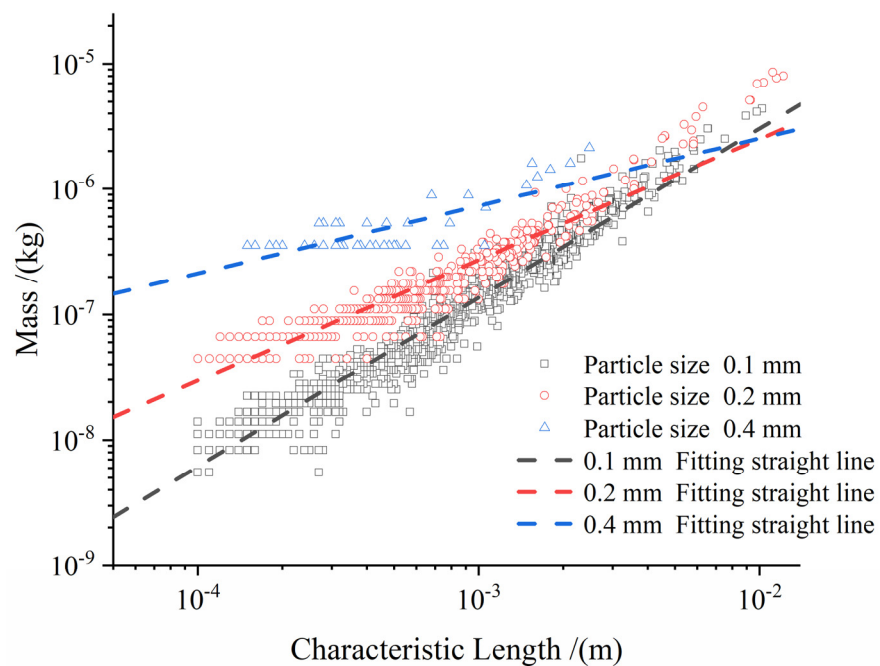


Figure 11. Characteristic length vs. mass under different particle sizes.

In conclusion, the SPH method can output more debris fragments, and the particle size has a great impact on the number of output fragments, the lower limit of statistical characteristic parameters and characteristic length parameters, but has little effect on the upper limit of fragment characteristic parameters and fragment mass. The characteristic length–mass relationship is greatly affected by the particle size when the characteristic length is in a small order of magnitude, and this effect decreases with increasing characteristic length. The fundamental reason is that the accuracy of characteristic length depends on the accuracy of the smallest particle. Generally, particles can be built with the size of

1/5~1/10 of the characteristic size of debris fragments to be studied. In addition, to study the law of characteristic parameters, after the particles are refined to a certain degree, the statistical law of each parameter becomes less affected by the particle size.

4.2.2. Finite Element Method-Smooth Particle Hydrodynamics Adaptive Coupling Algorithm

In the FEM-SPH adaptive coupling algorithm, considering the mesh scale limitation in preprocessing and computing software, the mesh sizes are set to 0.2, 0.4, and 0.8 mm. Similarly, to analyze the influence of mesh size on debris cloud calculation results in the adaptive coupling algorithm, it is necessary to compare the characteristic parameters of debris clouds at 6 μ s after impact under the three mesh sizes.

After the simulation conditions of the three mesh sizes are calculated, the contours of the debris clouds at 6 μ s are shown in Figure 12. The red particles in the debris cloud are produced by the aluminum alloy plate and the yellow particles are produced by the aluminum alloy ball. It can be roughly seen from these contours and section diagrams that in the FEM-SPH adaptive coupling method, large fragments are displayed in the form of finite elements and have clear physical boundaries, but the debris cloud is still composed of the SPH particles converted from failed material. In the initial modeling, the finer the mesh and the more the particles, the clearer the contour of the debris cloud, which allows for easier and more accurate statistical analysis of characteristic parameters. Moreover, it can be seen that the smaller the mesh size, the more the number of remaining fragments at the same moment. Some smaller fragments still exist in the form of finite elements, and the other data need to be measured accurately.

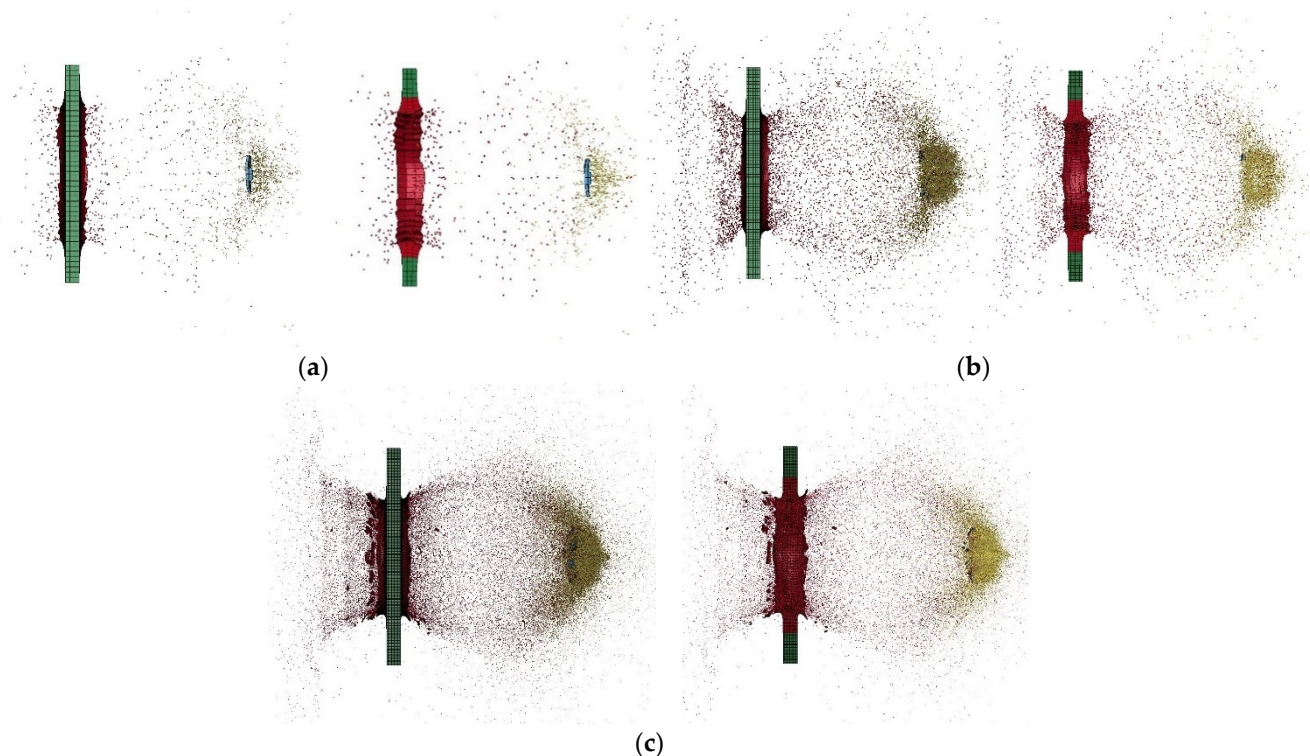


Figure 12. Contours and sections of debris clouds under different mesh sizes. (a) Particle size 0.8 mm; (b) particle size 0.4 mm; (c) particle size 0.2 mm.

Furthermore, to compare the stability of the calculation results of the characteristic parameters of the debris clouds under different initial mesh sizes, tools such as LS-PrePost are used, the characteristic parameter values under various simulation conditions are measured, and the change of each value is shown in Figure 13. From the observation of the curve smoothness, it is found that the distance h from the front end of the debris

cloud to the target plate and the value of the maximum diameter d_2 of the debris cloud are less sensitive to the mesh size, and the fluctuation does not exceed 0.4374 mm (<1.5%), but the perforation diameter d_1 is sensitive to the mesh size. As the mesh size increases, d_1 also gradually increases. When the mesh size is 0.8 mm, the perforation diameter is 3.15 mm (>15%) larger than that in the case of 0.2 mm. Regarding the ricochet angle and diffusion angle, except for the case of the 0.4 mm mesh size, the ricochet angle has a large decrease, and the change of the splash and diffusion angles in other simulation conditions is very small (<5%). Therefore, for the adaptive FEM-SPH coupling method, the initial mesh size has a relatively small effect on the overall contour of the debris cloud. Finally, regarding the three-stage velocity of the debris cloud, observing the trend of the curves, we can find that the initial mesh size has little effect on the velocity in the high-velocity and medium-velocity stages of the debris cloud but greatly affects the low-velocity stage. The velocity deviation in the high-velocity stage is $90 \text{ m}\cdot\text{s}^{-1}$, and that in the low-velocity stage is $520 \text{ m}\cdot\text{s}^{-1}$.

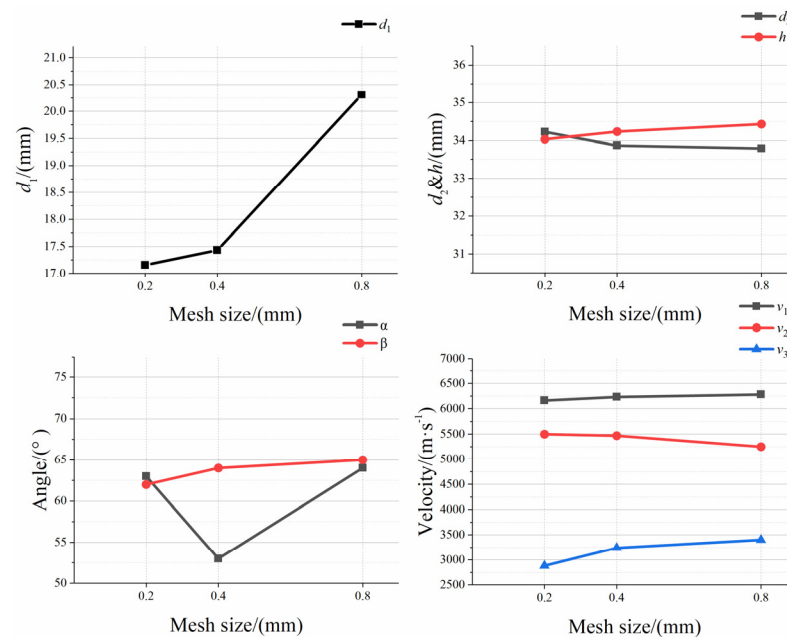


Figure 13. Curves of characteristic parameter values under different mesh sizes.

To sum up, the initial mesh size has little effect on the distance h from the front end of the debris cloud to the target plate, the maximum diameter d_2 of the debris cloud, the diffusion angle β , v_1 in the high-velocity stage, and v_2 in the medium-velocity stage, but has little effect on the perforation diameter d_1 , ricochet angle α of the debris cloud, and v_3 in the low-velocity stage.

Similarly, to analyze the influence of the initial mesh size on the calculation results of debris fragment characteristics, the characteristic parameters of the remaining debris fragments at $6 \mu\text{s}$ after impact under the mesh sizes of 0.2, 0.4, and 0.8 mm are studied and compared. As for the debris fragment distribution, according to the data output by LS-DYNA, the number of FEM fragments with clear boundaries obtained under the initial mesh sizes of 0.2, 0.4, and 0.8 mm are 95, 10, and 1, respectively. Therefore, the finer the initial meshes, the more the debris fragments obtained. The shape and approximate distribution of debris fragments are shown in Figure 14.

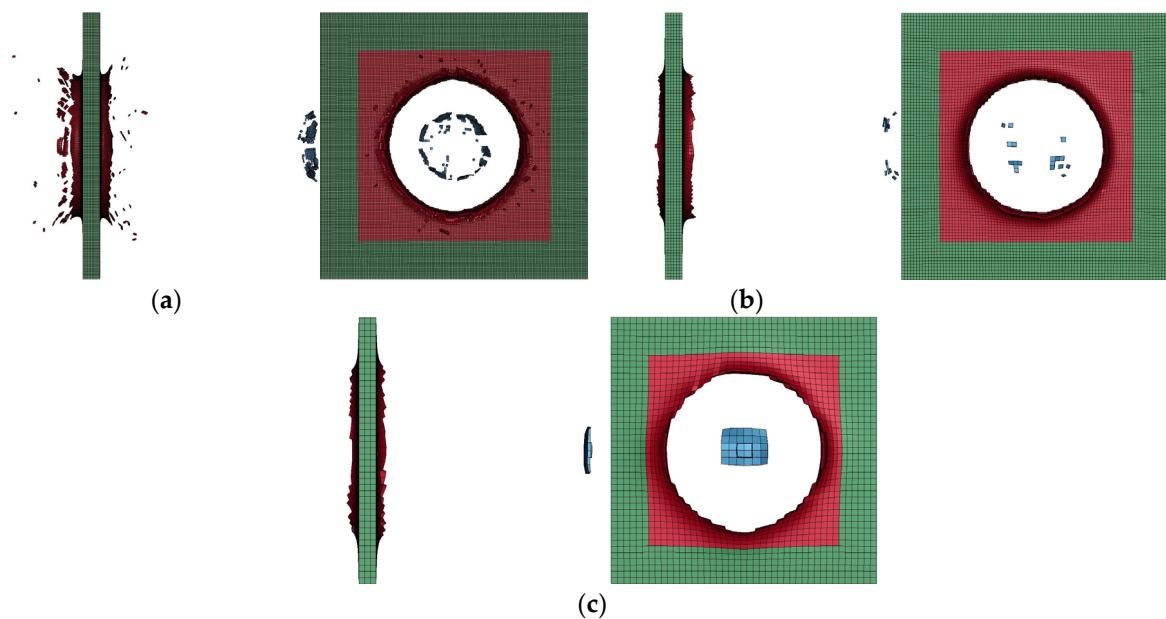


Figure 14. Schematic diagram of the shape and distribution of debris fragments under different mesh sizes. (a) Initial mesh size 0.2 mm; (b) initial mesh size 0.4 mm; (c) initial mesh size 0.8 mm.

Through the analysis of the FEM fragments in the FEM-SPH adaptive coupling method, it is found that although fragments with clear shapes can be obtained, too small fragments or those reaching the material failure conditions cannot be counted due to their conversion into the SPH particles. As a result, the total amount of debris fragments is smaller than the output in the SPH method. Test data are also needed to further verify the relationship between the statistical law obtained by the two methods and the real situation. On this basis, we further developed a debris fragment statistical program using the element and node data output by LS-PrePost and compared the fragment size distribution, mass distribution, and relationship between fragment mass and characteristic size under the 0.2 mm mesh size simulation condition (with a large number of fragments) and the three simulation conditions of the SPH method, as shown in Figure 15. From the trend of the curves, regarding the distribution law of characteristic length, the statistical law of the FEM-SPH method when the initial mesh size is 0.2 mm is very close to that of the SPH method when the particle size is 0.4 mm. In addition, similar to the SPH method, except for the deviation when the fragment data is composed of a single mesh, in general, the fragment characteristic length parameters obtained by the FEM-SPH method are linearly distributed in the logarithmic coordinate system, but the overall number is one order of magnitude less than that of the SPH particle simulation with the same accuracy.

Similarly, in the distribution statistics of fragment mass, although the mass distribution obtained by the FEM-SPH method is basically linear, there is a big gap in the number of fragments obtained by this method and SPH. The smaller the fragment mass, the greater the difference between the number of fragments output by the two simulation algorithms. Finally, in the statistical analysis of the relationship between the characteristic length and mass of fragments, as shown in the figure, the characteristic length–mass relationship obtained by both the FEM-SPH adaptive coupling method and the SPH method is linearly distributed in the logarithmic coordinate system. The linear functions obtained by fitting the condition of the particle size of 0.1 mm in the SPH method and the condition of the initial mesh size of 0.2 mm in the FEM-SPH method are shown in Equations (17) and (18). From the function expressions, we can see that the exponent of the function L_c fitted by the

simulation results of the FEM-SPH method changes from the SPH method's 1.3456 to 2.3370, which is closer to the exponent of the conventional hexahedron.

$$m_1 = 10^{-2.8279} \cdot L_c^{1.3456} \tag{17}$$

$$m_2 = 10^{0.4081} \cdot L_c^{2.3370} \tag{18}$$

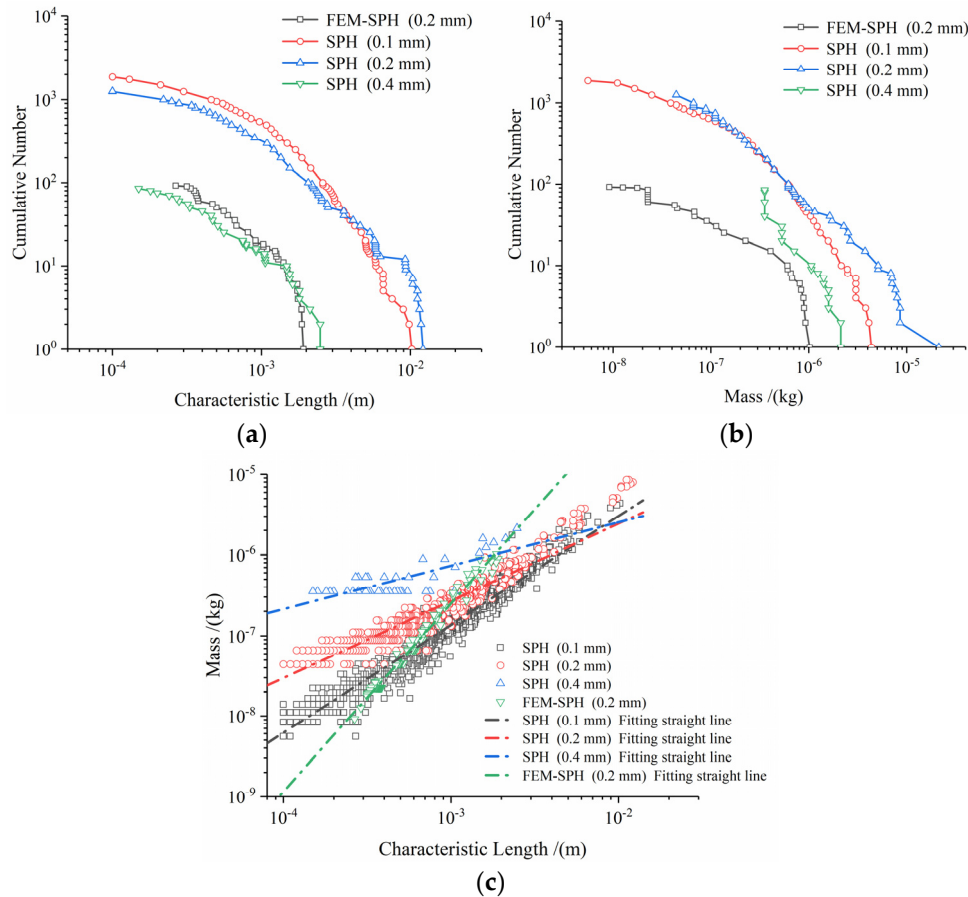


Figure 15. Comparison of fragment characteristic parameters between finite element method-smooth particle hydrodynamics and smooth particle hydrodynamics method. (a) Fragment characteristic length distribution; (b) fragment mass distribution; (c) fragment characteristic length vs. fragment mass.

4.2.3. Finite Element Method-Smoothed Particle Galerkin Fixed Coupling Algorithm

In the FEM-SPG fixed coupling algorithm, the mesh and SPG particle sizes are set to 0.2, 0.4, and 0.8 mm. To analyze the influence of the SPG particle size on the debris cloud calculation results, the characteristic parameters of the debris clouds at 6 μs after impact are compared. After the simulation conditions of the three particle sizes are calculated, the contour graphs of the debris clouds at 6 μs are shown in Figure 16. According to these contour graphs, when the effective plastic strain is used as the failure criterion of bonds between SPG particles, the response of the impact surface of the aluminum plate and the shape of the debris cloud are irrational. As the particles become finer, the particles of the aluminum projectile in the debris cloud tend to concentrate more on the front, and the deviation between the debris cloud and its conventional form grows larger. Moreover, similar to the SPH method, the fragments produced in the SPG method have no clear boundaries, and there is no method to output fragment data of the SPG particles, which makes it difficult to use the FEM-SPG fixed coupling method to make subsequent statistical analysis of debris fragments.

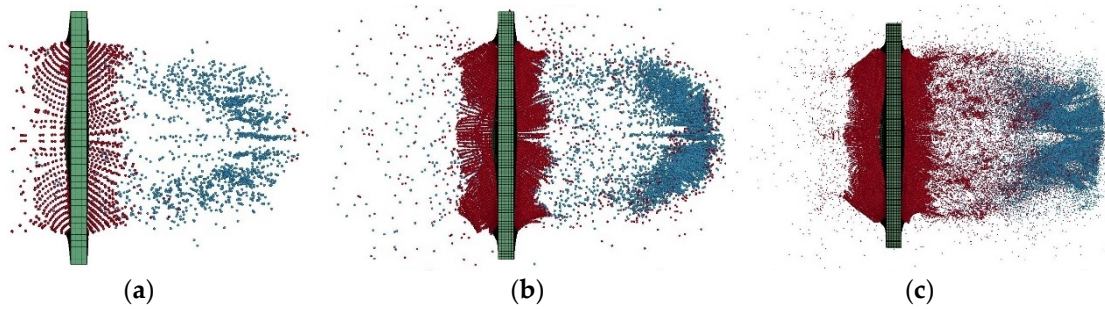


Figure 16. Contour graphs of the debris clouds under different particle sizes. (a) Particle size 0.8 mm; (b) particle size 0.4 mm; (c) particle size 0.2 mm.

To compare the stability of the calculation results of the debris cloud characteristic parameters under different SPG particle sizes, LS-PrePost is used to measure the characteristic parameter values under the three simulation conditions, and the change in each value is shown in Figure 17. Observing the change in the curves, we can find that in the FEM-SPG method, the perforation diameter d_1 , the maximum diameter of the debris cloud d_2 , and the distance h from the front end of the debris cloud to the target plate in the simulation results are all greatly affected by the particle size, and the changes are 1.8122 mm (>9%), 2.7252 mm (>9%), and 2.3717 mm (>7%), respectively. Furthermore, the ricochet angle and diffusion angle of the debris cloud also vary significantly. The diffusion angle is even close to or greater than 90° . Therefore, for the SPG method, the obtained shape of the debris cloud is different from other algorithms. Finally, the three-stage velocity of the debris cloud also has certain instability as the particle size changes. The velocity changes in the high- and medium-velocity stages are small, within $600 \text{ m}\cdot\text{s}^{-1}$, while the velocity change in the low-velocity stage is large, which can reach $990 \text{ m}\cdot\text{s}^{-1}$.

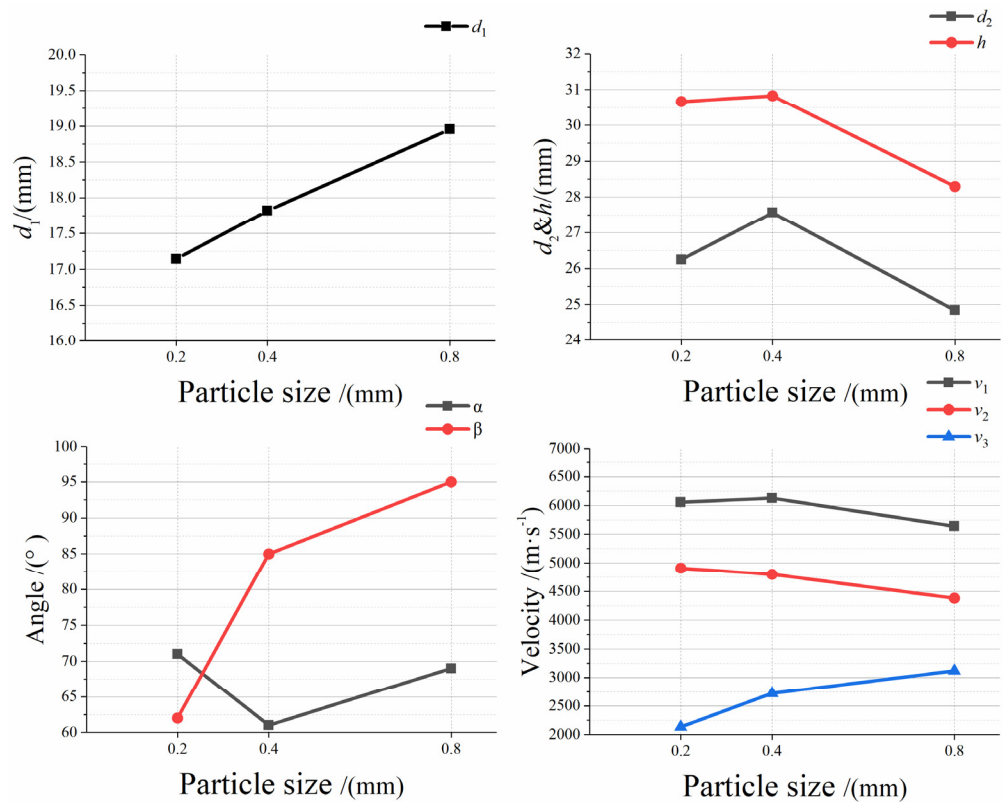


Figure 17. Curves of characteristic parameter values under different particle sizes.

In summary, through the calculation of the FEM-SPG method, the particle size has a relatively large impact on all the characteristic parameters of the debris clouds. The biggest problem with this algorithm is that the shape of the debris cloud is different from the conventional situation, and there is no effective statistical method for the debris fragments.

4.2.4. Node Separation Algorithm

In the node separation algorithm, due to the limitation of the number of meshes on the running time of the node group program, the mesh sizes are set to 0.4 and 0.8 mm. At the beginning, the characteristic parameters of the debris clouds at 6 μ s after impact under the two mesh sizes are compared. After the two simulation conditions are calculated, the contour graphs of the debris clouds at 6 μ s are shown in Figure 18.

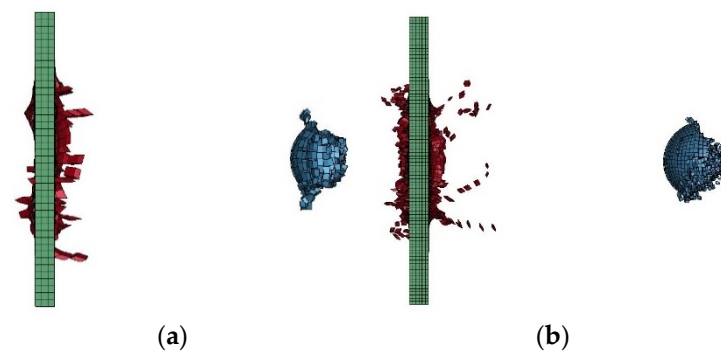


Figure 18. Debris cloud contours under different mesh sizes. (a) Mesh size 0.8 mm; (b) mesh size 0.4 mm.

The simulation results show that although the node separation method can ensure that all fragments are composed of FEM meshes and have clear physical boundaries, it also has obvious shortcomings in dealing with hypervelocity impact problems. If the material has a corresponding failure model, it is difficult to form a complete debris cloud via this method, and the aluminum projectile cannot produce fragments effectively. When the ratio of single-layer plate thickness to mesh size is 5, the node separation algorithm cannot well simulate the hypervelocity impact scenario. However, it can also be seen from the figure that when the mesh size decreases from 0.8 mm to 0.4 mm, the shape of the debris cloud is improved. Due to the limitations of mesh scale and the efficiency of node group programming, more studies need to be done to make clear whether the node separation algorithm is suitable for hypervelocity impact analysis.

In this algorithm, although the debris cloud is incomplete and not all the characteristic parameter values can be obtained, most of the data can be measured by LS-PrePost, as shown in Table 4, where data about the maximum diameter of the debris cloud d_2 , the ricochet angle α , and the diffusion angle β is incomplete. Among the other parameters, the perforation diameter d_1 and the distance h from the front end of the debris cloud to the target plate are greatly affected by the particle size, while the velocities in the three velocity stages of the aluminum projectile have a small difference, and the maximum velocity difference is $30 \text{ m}\cdot\text{s}^{-1}$ (<5%).

Table 4. Characteristic parameters of debris clouds under different mesh sizes by node separation method.

Mesh Size	d_1 (mm)	h (mm)	v_1 ($\text{m}\cdot\text{s}^{-1}$)	v_2 ($\text{m}\cdot\text{s}^{-1}$)	v_3 ($\text{m}\cdot\text{s}^{-1}$)
0.4 mm	12.587	35.238	6580	6490	6550
0.8 mm	14.235	33.973	6570	6520	6520

To sum up, regarding the difference in calculation accuracy of the four algorithms under different mesh sizes, through the above analysis and comparison, it is found that: (1) As

for the calculation results of the debris clouds, although the node separation method can display more complete debris clouds with decreasing mesh size, limited by the mesh scale limit in the existing calculation, it cannot display the shape of the debris clouds completely. In addition, according to the calculation results by the FEM-SPG fixed coupling method, the particle size has a great influence on all characteristic parameters of the debris clouds. Although the debris clouds can be obtained via this method, their shapes are different from the conventional situation. Both the FEM-SPH adaptive coupling method and the SPH method can obtain better debris cloud shapes, and the characteristic parameters of the debris clouds obtained by the FEM-SPH adaptive coupling method are generally lower than those by the SPH method due to the effect of the mesh size. (2) As for the calculation results of debris fragment characteristics, in the hypervelocity impact problems, the aluminum projectile (impactor) cannot be broken into fragments effectively. Moreover, the FEM-SPG fixed coupling algorithm has no mature statistical method for the data of debris fragments. Both the FEM-SPH and SPH methods have the problem that the information on debris fragment characteristic parameters, including the number of fragments, the lower limit of statistical characteristic parameters, and the characteristic length parameter, is greatly affected by the particle size. On the other hand, the SPH method cannot output debris fragments with clear physical boundaries, which significantly affects the subsequent reentry analysis of the debris fragments in the analysis of hypervelocity impact on spacecraft. However, although the FEM-SPH method can obtain fragments with clear shapes, too small fragments or those reaching the material failure conditions cannot be counted due to their conversion into the SPH particles, resulting in the total amount of fragments, especially the small-mass fragments, lower than the output of the SPH method. In addition, the index of the linear function L_c of the characteristic length and mass fitted by the FEM-SPH method is closer to the index of the volume of the conventional hexahedron. Finally, as for the accuracy of the calculation results of the debris fragment characteristic parameters by the two simulation algorithms, more test data is needed to further verify the relationship between the statistical law obtained by the two methods and the real situation.

4.3. Comparative Analysis of Simulation Results Accuracy of the Four Algorithms

After obtaining the sensitivity of the four algorithms to the mesh, it is necessary to further study the accuracy of each algorithm. First, based on the exact solution, the correctness of the running and parameter setting of the numerical simulation software is verified. Secondly, the simulation results of different numerical algorithms are compared with the experimental data of the same impact conditions, and the accuracy of the mathematical model of the simulation algorithm is compared and verified. Finally, for the calculation results of each algorithm and mesh size, the cumulative error caused by the number of integration steps is estimated.

4.3.1. Comparison and Analysis of Simulation Result Accuracy of Four Algorithms Based on Exact Solution

When the accuracy of the calculation results of the four numerical simulation algorithms is being analyzed, the simulation results of the characteristic parameters with accurate or analytical solutions are primarily compared with the results of the theoretical formula. Specifically, for the basic research problems in the field of hypervelocity impact of a spherical projectile on a single-layer plate, there are generally four characteristic parameters that can be accurately solved by empirical, semi-analytical, and analytical formulas. These parameters are the characteristic parameters describing the motion of debris cloud, namely, head velocity v_1 , interface velocity v_2 , and tail velocity v_3 , as well as the characteristic parameter describing the damage of the hypervelocity impact target, namely, perforation diameter d_1 .

Bless [40] proposed a debris cloud model by theoretical derivation based on a large number of the test results of Piekutowski [41], and obtained three axial characteristic parameters that can be used to describe the movement of debris cloud through one-dimensional

shock wave theory, namely, head velocity v_1 , interface velocity v_2 and tail velocity v_3 . According to the theory of shock wave in solid in the field of hypervelocity impact, the qualitative analysis results show that a strong shock wave is formed in the projectile and the target plate after impact. According to the one-dimensional shock wave theory, the particle velocity difference u in front of and behind the shock wave front can be obtained, as shown in Formula (19).

$$u = v_0 \left\{ 1 + \left[\frac{\rho_{0b}(1 - \rho_{0p}/\rho_{1p})}{\rho_{0p}(1 - \rho_{0b}/\rho_{1b})} \right]^{1/2} \right\}^{-1} \quad (19)$$

where v_0 is the initial impact velocity, ρ_{0b} and ρ_{1b} are the density of the target before and after the impact, respectively. Moreover, ρ_{0p} and ρ_{1p} are the density of the projectile before and after impact, respectively.

The particle velocity in the target is u and that in the projectile is $(v_0 - u)$ after the shock wave impact. Under the influence of sparse waves, the pressure in the material is unloaded to zero and the material further accelerates. The expressions of v_1 , v_2 , and v_3 can be obtained using one-dimensional shock wave theory as follows.

$$v_1 = 2u \quad (20)$$

$$v_2 = 2u - v_0 \quad (21)$$

$$v_3 = u \quad (22)$$

The above is the Bliss model describing the movement of debris cloud deduced from the one-dimensional shock wave theory. The velocity calculated by this model is in good agreement with the experimental result of a cylindrical projectile, while the coincidence degree of a spherical projectile is modest. Therefore, the Bliss model and benchmark experimental values can be used in combination as the exact solution of debris cloud expansion velocity to verify the accuracy of debris cloud velocities calculated by different numerical simulation methods.

Since the 1960s, scholars outside China have developed a series of empirical and semi-empirical models for analyzing the perforation diameter of thin plates impacted by a spherical projectile at hypervelocity based on the principle of mechanics and the regression analysis of their experimental data. The most representative models for analyzing hole diameter include the Swale, Hill, Hosseini, and Chant models. In these models, only the Chant model is based on basic hydrodynamics principles and empirical constants without relying on experimental data. Therefore, the Chant [42] Formula (23) is selected to calculate the accurate solution of perforation diameter.

$$\frac{d_1}{d_p} = \sqrt{2\pi} \left[\left(\frac{\rho_p}{\rho_t} \right) \left(\frac{v}{c_t} \right) \right]^{0.5} \left(\frac{T_t}{d_p} \right) + 1.0 \quad (23)$$

where d_1 is the projectile perforation diameter, d_p is the projectile diameter, and v is the projectile impact velocity, ρ_t is the target density, ρ_p is the projectile density, c_t is the sound velocity in the target material, and T_t is the thickness of the target plate.

From the above analysis, the relevant parameters regarding aluminum ball hypervelocity impact are put into Formulas (19)–(23), and the following exact solutions are obtained: head velocity $v_1 = 5929.52 \text{ m}\cdot\text{s}^{-1}$, interface velocity $v_2 = 5936.16 \text{ m}\cdot\text{s}^{-1}$, tail velocity $v_3 = 3559.04 \text{ m}\cdot\text{s}^{-1}$, and perforation diameter $d_1 = 20.884 \text{ mm}$.

It can be known from the previous analysis that the FEM-SPG fixed coupling and the node separation algorithms cannot completely or accurately depict the shape of the debris cloud, therefore these algorithms are not suitable for hypervelocity impact kinetic energy damage in terms of the macroscopic algorithm. In light of this, this study aims to analyze the problems in the simulation results by comparing the exact solutions of hypervelocity

impact characteristic parameters. The comparison between the SPH method, the FEM-SPH adaptive coupling method, the FEM-SPH fixed coupling method, and the node separation method in terms of the difference between the simulated results and the exact solutions with different mesh sizes is shown in Figure 19.

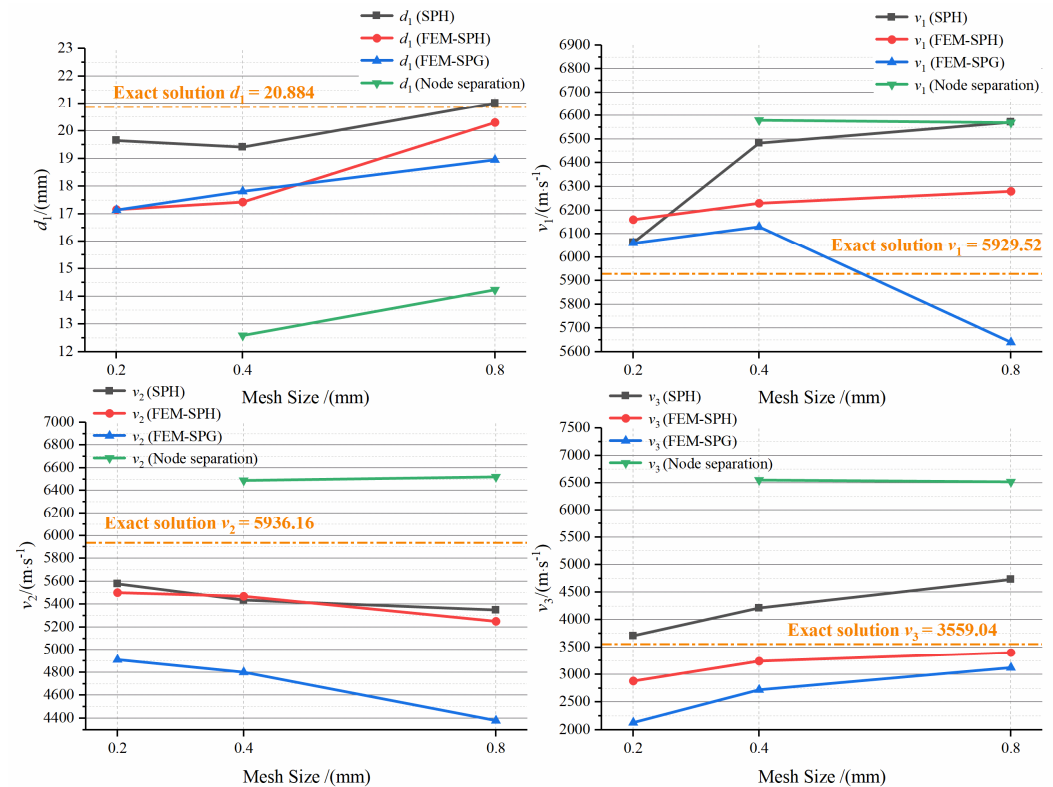


Figure 19. Comparison between the simulation results and the exact solutions of hypervelocity impact characteristic parameters.

As can be seen from Figure 19, for the perforation diameter d_1 , the error between the numerical calculation results and the exact solution of the SPH, the FEM-SPH, and the FEM-SPG algorithms are less than 20%, which is acceptable for the characteristic parameters of the target plate damaged by kinetic energy in an impact. However, the deviation between the results calculated by the node separation algorithm and the exact solution is too large. Therefore, the settings of the node separation algorithm adopted by the K file and the mesh parameters in this paper is not suitable for hypervelocity impact analysis. Moreover, regarding the three velocity characteristic parameters of debris cloud motion, it can be seen from the figure that considering the deviation from the exact solution for the three parameters, the FEM-SPH adaptive coupling algorithm shows the smallest combined error, which is within 5%. The deviation between the head velocity calculated by the SPH algorithm and the exact solution is too large, while the interface velocity calculated by the FEM-SPG algorithm is far smaller than the exact solution.

Based on the exact solution, the correctness of the running and the parameters setting of the numerical simulation software is verified and analyzed. The keyword, parameters setting, and running results of the numerical simulation software show that the node separation algorithm is not suitable for hypervelocity impact analysis using the current K file parameters and mesh setting. In comparison, the SPH, the FEM-SPH, and the FEM-SPH numerical simulation methods show better calculation results for the hypervelocity impact process. Moreover, the total error between the numerical results obtained by the FEM-SPH adaptive coupling algorithm and the exact solution is the smallest, which meets the error criterion of numerical simulation of impact kinetic energy damage.

4.3.2. Comparison of Simulation Results of Four Algorithms Based on Experimental Data

Based on the comparative analysis of the simulation results obtained from the four simulation algorithms and the theoretical results for the characteristic parameters with accurate or analytical solutions concerning the hypervelocity impact of spherical projectiles on single-layer plates, the running of software and parameter settings is verified. In addition, the calculation results of different numerical algorithms are compared with the experimental results under the same impact conditions, and the accuracies of these algorithms are compared. Therefore, the calculation results of each algorithm need to be compared with Piekutowski's test results [34,35]. The photos of debris clouds and the perforation diameter in the test are shown in Figure 20.

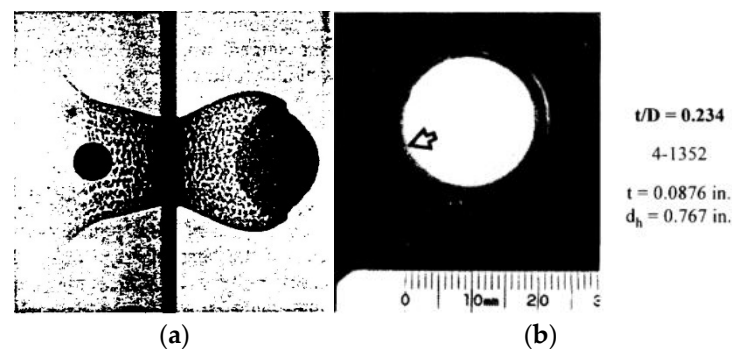


Figure 20. Photos of Piekutowski's test [34,35]. (a) Debris cloud photo in 4-1352 test; (b) perforation diameter photo in 4-1352 test.

From the recorded test data and the proportion of the debris cloud photos, the test data of debris cloud characteristic parameters are obtained using tools such as GetData, as shown in Table 5.

Table 5. Characteristic parameter data of debris clouds in Piekutowski's test.

Test No.	d_1 (mm)	d_2 (mm)	h (mm)	α (°)	β (°)
4-1352	19.4818	34.8517	34.3049	72	64

The comparison of the debris cloud appearances obtained by the four methods is shown in Figure 21. As illustrated, in terms of the accuracy and integrity of debris cloud contours, the FEM-SPG fixed coupling method and node separation method are not suitable for hypervelocity impact analysis at present. The SPH and FEM-SPH adaptive coupling methods give results similar to the debris clouds obtained by the test, with the former performing better, but the accuracy of the characteristic parameters calculated by the two methods needs to be further compared.

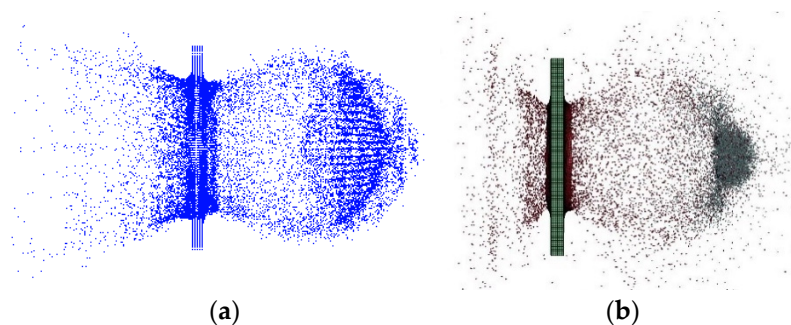


Figure 21. Cont.

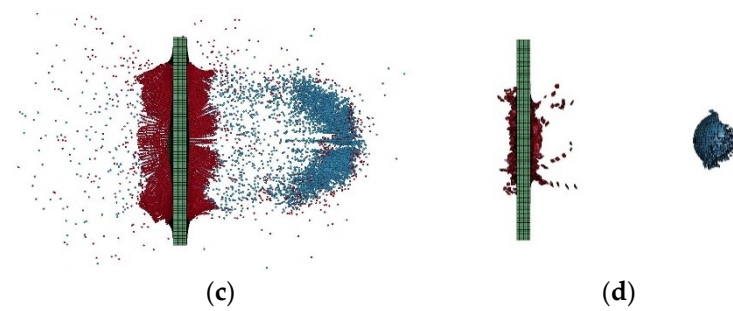


Figure 21. Comparison of simulation effects of debris clouds. (a) Debris cloud of the smooth particle hydrodynamics method; (b) debris cloud of the finite element method-smooth particle hydrodynamics adaptive coupling method; (c) debris cloud of the finite element method-smoothed particle Galerkin fixed coupling method; (d) debris cloud of the node separation method.

In terms of accuracy, the SPH and FEM-SPH adaptive coupling methods are compared with the test results under different mesh sizes, as shown in Figure 22.

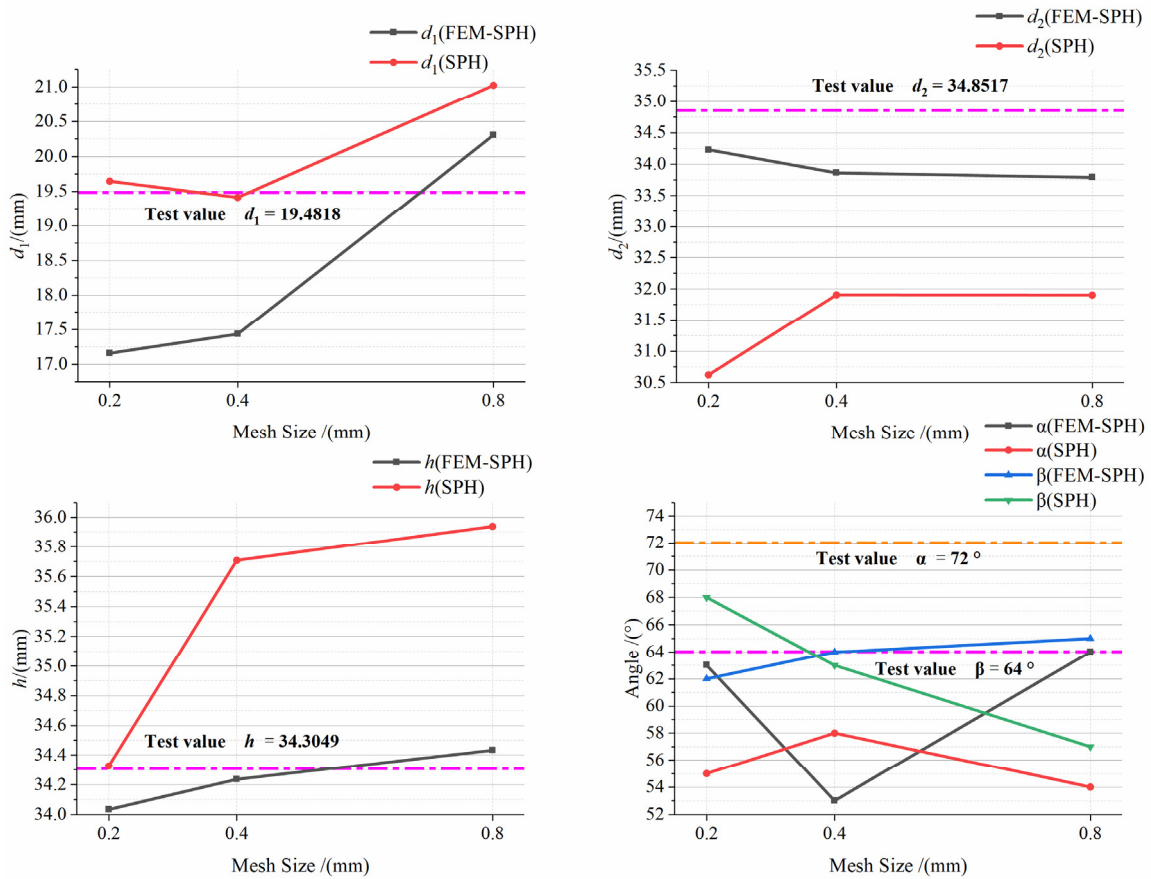


Figure 22. Comparison of simulation data and test data of debris cloud characteristic parameters.

According to the figure, only the perforation diameter d_1 of the SPH method is closer to the corresponding test value, and all the other geometric characteristic parameters of the debris clouds of the FEM-SPH method are closer to their test values. The comparison is presented in Figure 23.

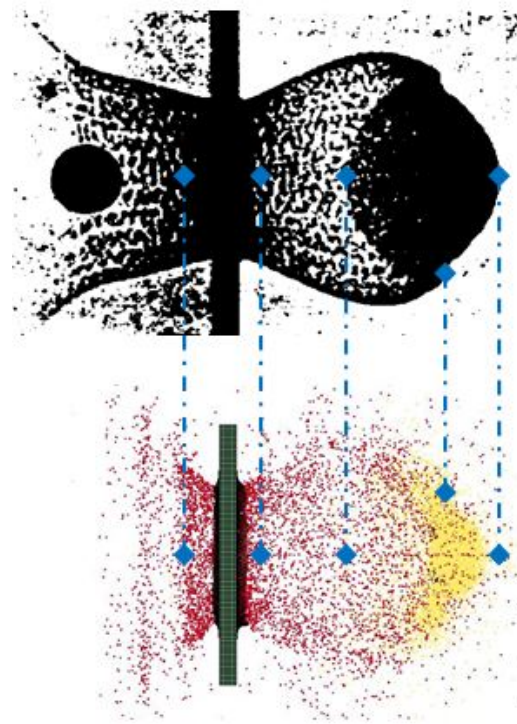


Figure 23. Comparison of simulation and test data of debris cloud characteristic parameters.

4.3.3. Precision Estimates

From the accuracy analysis of the numerical algorithms based on the exact solution and experimental data, it is found that the calculation results of the FEM-SPH adaptive coupling algorithm show the best agreement with the exact solution and experimental data, and the error is mostly less than 5%. It can be seen that the mathematical model of the algorithm itself, the keywords, and parameter settings of the current K file and the running of the software are correct and are most suitable for the analysis of hypervelocity impact. On the other hand, there still exist random errors on the same order of magnitude due to different spatial resolutions and integration accuracies, although the study of the selected method and solver is not a systematic error. When summarizing the random error of continuous time steps, it can be found that the integral error is proportional to the square of the number of time steps, which slows the error accumulation. However, this error still exists and should be evaluated in each numerical simulation [43].

Smirnov evaluated the accuracy of numerical simulation of the unsteady process and introduced the reliability parameter R_s that represents the maximum permitted time step to ensure the random error accumulation does not exceed a given value. The specific expression of R_s can be summarized in Formula (24) [44].

$$R_s = \frac{n_{\max}}{n} = \frac{\left(S_{\max} / \sum_{i=1}^3 \left(\frac{1}{N_i} \right)^{k+1} \right)}{n} \quad (24)$$

where S_{\max} is the maximum allowable total error, N_i is the number of elements in the direction of integration, k is the order of numerical format accuracy, n is the time steps of integration, and n_{\max} is the maximum allowable time steps. The ratio (24) represents the reliability of the result, which indirectly reflects the accumulated error. It can be seen from the expression that the higher the value of N_i , the smaller the value of n , the higher the value of R_s , and the smaller the error. As R_s shifts towards 1, the accumulated error tends to the maximum allowable value.

Table 6 summarizes the accumulated errors of the FEM-SPH numerical simulation method with the highest overall numerical calculation accuracy with different mesh sizes.

The allowable error S_{\max} is assumed to be 5%. It can be seen from the table that the error accumulation speed of coarse mesh is high, but it decreases with the increase in mesh resolution. Therefore, for the current simulation, all the results indicate that the software and the FEM-SPH adaptive coupling algorithm are highly reliable.

Table 6. Error estimates.

Numerical Algorithm	Allowable Error/(%)	Grid Resolution	Physical Time Simulated /(μ s)	Number of Time Steps	Accumulated Error	Allowable Number of Time Steps	Reliability (R_s)
FEM-SPH	5	232 × 232 × 68	6	8465	0.0003073	2.241 × 10 ⁸	26,474
		116 × 116 × 34		3907	0.001670	3,500,552	896
		58 × 58 × 17		1874	0.009255	54,697	30
SPH		232 × 232 × 68		610	0.006259	38,927	64
		116 × 116 × 34		311	0.017877	2432	8
		58 × 58 × 17		152	0.049990	152	1

To sum it up, regarding the analysis of debris cloud characteristics, the accuracy of four different numerical simulation algorithms is compared and analyzed from the perspectives of mesh sensitivity, the difference between the numerical simulation results and exact solutions, the difference between the numerical simulation results and the experimental ones, and the accumulated error analysis. It is found that the FEM-SPH adaptive coupling algorithm is more suitable for the hypervelocity impact of large-scale complex structures. From the perspective of mesh sensitivity and accuracy of debris fragment characteristic parameters, the SPH and FEM-SPH methods have high mesh sensitivity in debris fragment output, while the SPH method can output a large number of debris that can be used for statistics, but they do not have clear physical boundaries and shapes, which greatly impacts subsequent research. Therefore, from the perspective of debris fragments, it is preferred to use the FEM-SPH adaptive coupling method to simulate the hypervelocity impact on full-scale complex structures. This requires the determination of the relationship between the debris fragment output by the FEM-SPH method and the real test data.

5. Verification of Space Debris Impact Satellite Simulation

Through the study of four algorithms under the simulation conditions of different mesh/particle sizes based on the test of aluminum projectile impact on aluminum plate, it is found that the simulation results of the FEM-SPH adaptive coupling method are relatively less sensitive to the mesh size, and are closer to the real test values, making it more suitable for the simulation of hypervelocity impact on full-scale complex structures. However, there is still a lack of test verification of the distribution law of debris fragment characteristic parameters, which is a concern in the follow-up research. Therefore, the simulation condition TEST C in the characteristics study of debris fragments from satellite breakup due to hypervelocity impact by Liu Sen is selected as the simulation condition for verification [28].

5.1. Establishment of Simulation Model of Satellite for Verification

The parameters set by Liu Sen in the test are shown in Table 7, where the subscript p represents space debris and the subscript t represents the simulated satellite. Based on the setting of test conditions, the simulation structure model and parameters are determined. The thickness of the satellite's bottom plate, side plates, inner diaphragm, and connecting parts is 2 mm [29], and the material is 2024 aluminum alloy with a density of 2780 kg·m⁻³. The thickness of the central cylinder of the satellite is 1.5 mm and its material is 2024 aluminum alloy. The sizes of the electronic box on the satellite diaphragm are 10 mm × 5 mm × 3.5 mm and 15 mm × 5 mm × 3.5 mm with a thickness of 1.5 mm. The material is 6063 aluminum alloy, which is commonly used for electronic boxes, with

a density of $2700 \text{ kg}\cdot\text{m}^{-3}$. The space debris is equivalent to the shape of a projectile. Its structure consists of a 13 mm hemisphere, a 10 mm cylindrical section, and a 35 mm hollow circular platform section. Its material is 6061 aluminum alloy with a density of $2700 \text{ kg}\cdot\text{m}^{-3}$.

Table 7. Comparison test parameters [36].

Test No.	$\Phi_p/(\text{mm})$	$L_p/(\text{mm})$	$M_p/(\text{g})$	$L_t/(\text{mm})$	$M_t/(\text{g})$	$V/(\text{km}\cdot\text{s}^{-1})$
Test C	41	58	97.64	400	7295	3.26

After the simulation model is established according to the above parameters, through calculation, the overall dimension of the satellite model is $400 \text{ mm} \times 400 \text{ mm} \times 400 \text{ mm}$, total mass $M_t = 7338.515 \text{ g}$, and simulated projectile mass $M_p = 98.706 \text{ g}$. The simulated complex satellite structure and the electronic box as well as their simulation models are shown in Figure 24.

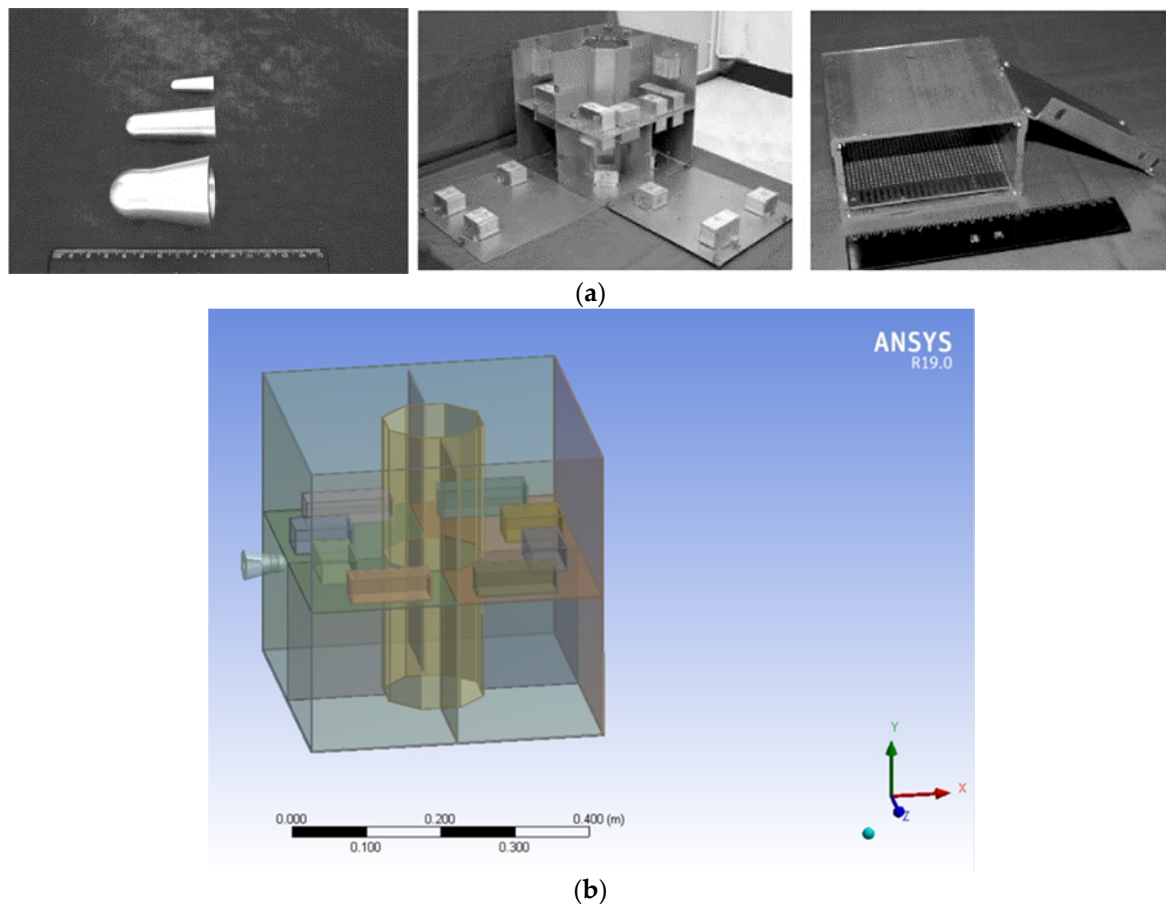


Figure 24. Schematic diagram of physical objects and simulation models of the simulated complex satellite structure and projectile. (a) Projectile, simulated complex satellite structure, and electronic box; (b) schematic diagram of the simulation structures of the projectile and simulated complex satellite structure.

When we set the mesh size, according to the previous conclusions, although the characteristic parameters of debris clouds are minorly affected by the mesh size when using the FEM-SPH adaptive coupling method, accumulated error and the effective statistical number of debris fragments are greatly affected by it, and the fragment data near the minimum mesh size is distorted to a certain extent. Therefore, when meshing for the model of space debris impact on simulated satellite, the mesh scale is set to the maximum amount that the pre-processing software can handle, namely, 2 mm [9]. The meshing

for hypervelocity impact on the simulated satellite by the projectile using the FEM-SPH method is shown in Figure 25.

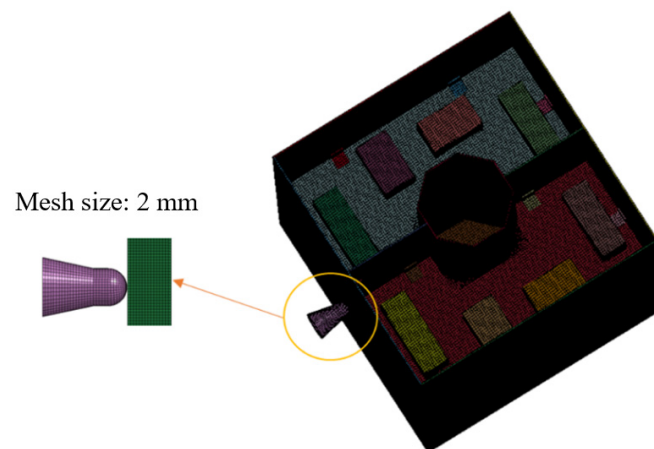


Figure 25. Schematic diagram of meshing for the model of projectile impact on simulated satellite by finite element method-smooth particle hydrodynamics method.

When we set the FEM-SPH adaptive coupling method keyword for the calculation example of space debris equivalent projectile impact on the simulated satellite, the basic setting is similar to that of the test of aluminum projectile impact on aluminum plate, but the contact setting is changed from a simple structure to a complex structure. For the projectile and the satellite, the keyword `*CONTACT_ERODING_SINGLE_SURFACE` is set to automatically identify the erosion contact between the surfaces. The static friction coefficient is set to $f_s = 1.05$ and the dynamic friction coefficient $f_d = 1.40$ for the aluminum alloy materials. In addition, due to the high impact velocity of the hypervelocity problem, the meshes of the contact surfaces of the two impactors can easily penetrate each other, and as the impact position is where multiple satellite plate structures converge, the parameters `SOFT = 2` and `DEPTH = 5` are set in Optional Card A to prevent penetration between different parts and elements.

5.2. Suitability Analysis of the Finite Element Method-Smooth Particle Hydrodynamics Adaptive Coupling Numerical Simulation Algorithm for Asymmetric Spacecraft Target

Due to the existence of stiffeners, bolts, and structures alike, the metal targets on the spacecraft rarely affect each other in a cylindrical symmetrical way from all directions. Therefore, it is necessary to evaluate the suitability of the FEM-SPH method to non-symmetric targets. During the breakup of the satellite, the effect of space debris impact on non-symmetric targets is reflected in the change of the impact position, making it far away from the center of the impact surface. Therefore, the structural asymmetry is treated equivalently as the shift of the initial impact position of the spherical projectile while keeping the other conditions unchanged, and the suitability of the FEM-SPH method to the calculation of the breakup of the established satellite large-scale target is studied. The specific settings of the numerical simulation are shown in Table 8. The ratio of the horizontal distance between the projectile center and the satellite geometric center to the half side-length of the satellite is defined as Δ .

Table 8. Simulation conditions.

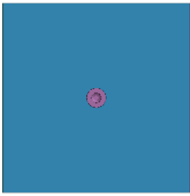
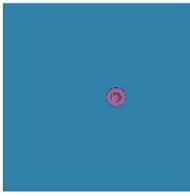
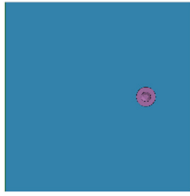
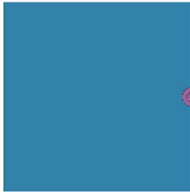
No.	Test C	Non-Symmetry 1	Non-Symmetry 2	Non-Symmetry 3
Δ (%)	0	20	50	100
Schematic				

Figure 26 shows schematics of the breakup of satellite 265 μ s after the hypervelocity impact of space debris at four different positions on a large-scale simulated satellite. By analyzing the macroscopic damage and the stress diagram, it can be seen that when hitting a non-symmetric target, the change in the impact position not only results in the changes in space debris and components and structures in the satellite impact channel but also leads to different overall damage and breakup effects of the satellites. Through the same period of time after impact, the structural plates show different extents of disintegration. In the case of $\Delta = 0\%$, the disintegration of the satellite plates is the least serious. Furthermore, for fragment projectile hypervelocity impact, the peak value of the stress response of the satellites is basically the same, the stress concentration phenomenon can be observed around the perforation and the connecting parts. In addition, the mechanical responses of the target structure in the impact channel and its vicinities are more obvious. Therefore, the FEM-SPH adaptive coupling algorithm is suitable for the simulation of the hypervelocity impact of non-symmetric targets.

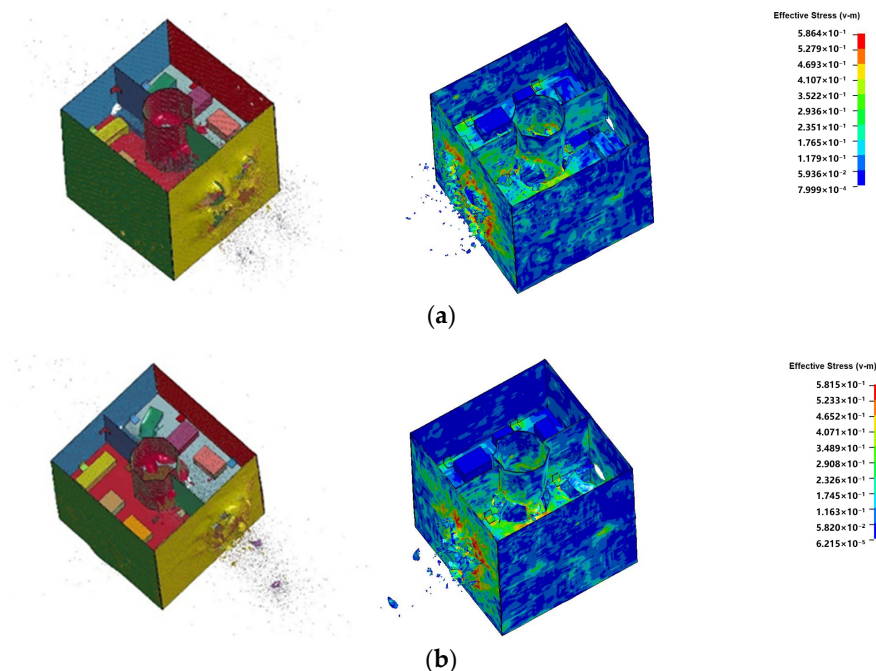


Figure 26. Cont.

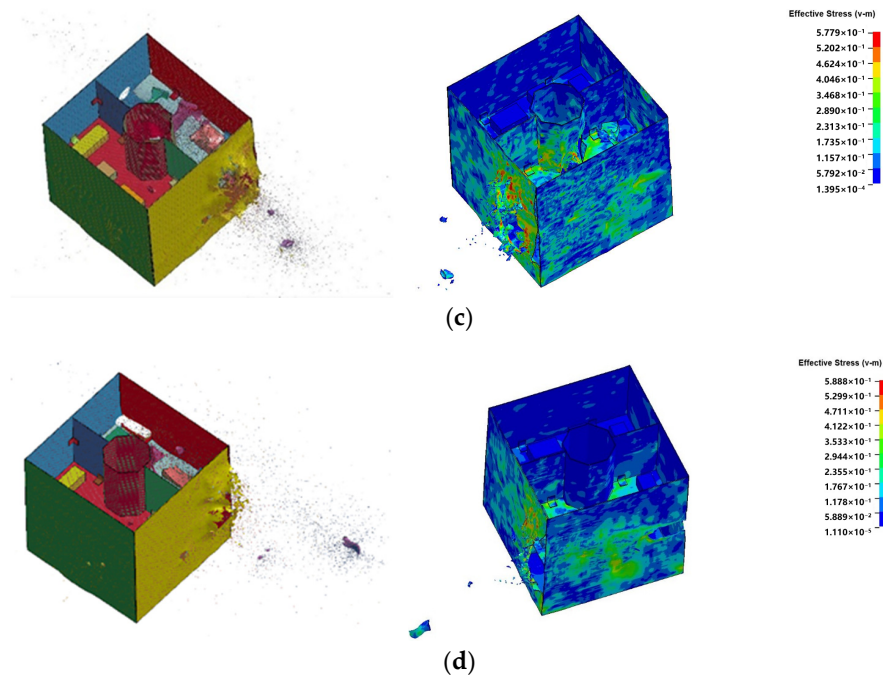


Figure 26. Schematics showing the disintegration of the simulated large-scale satellites 265 μ s after the impact with the hypervelocity space debris at four different positions. (a) Test C ($\Delta = 0\%$); (b) non-symmetry 1 ($\Delta = 20\%$); (c) non-symmetry 2 ($\Delta = 50\%$); (d) non-symmetry 3 ($\Delta = 100\%$).

5.3. Comparison and Verification of Algorithm Accuracy Based on Test

Firstly, with regard to the study of hypervelocity impact on spacecrafts such as satellites, the focus is often on macroscopic phenomena such as spacecraft breakup and damage after impact. Therefore, the simulation process of simulated satellite breakup and damage by the FEM-SPH adaptive coupling method and the similarity of the damage effect graphs with the test results are compared firstly, so as to judge the calculation accuracy of the algorithm for such macroscopic events as breakup. The comparison of the simulation and test of the overall breakup and structural component damage is shown in Figure 27.

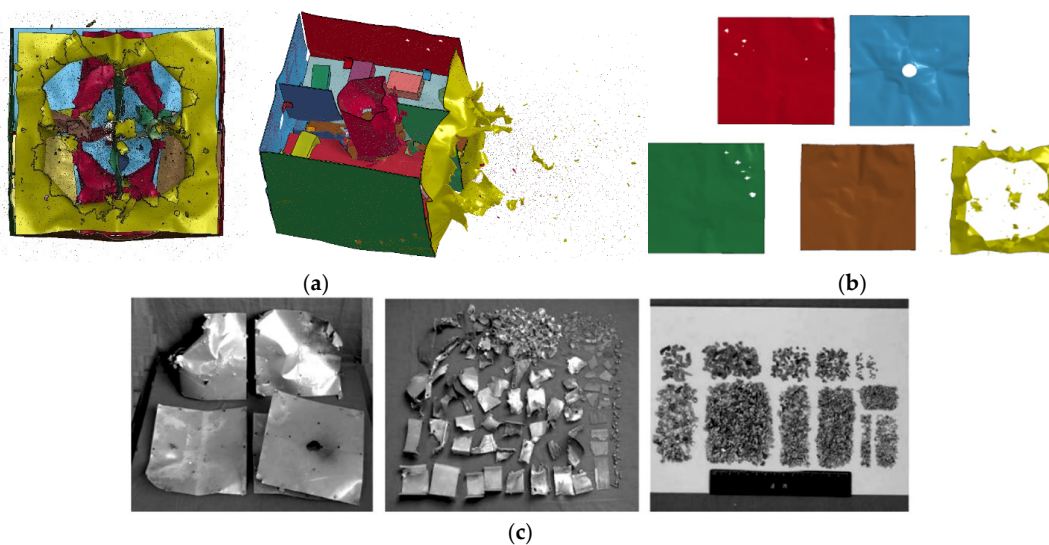


Figure 27. Comparison of satellite's overall breakup and structural component damage between simulation and test. (a) Simulation graphs of the overall breakup of satellite; (b) simulation graph of damage of satellite's structural components; (c) test photos of satellite's overall breakup and structural component damage [36].

As is seen from Figure 27, the connection between the main structures of the satellite has been damaged, the main five aluminum plates of the main structure completely separated, the simulated electronic box near the impact area also damaged to varying degrees, and the inner diaphragm and central cylinder structure of the satellite also damaged. The simulation conditions for complete breakup are the same as in the conclusion of complete breakup obtained in the test. In addition, in the simulation, the corners of the five aluminum plates are deformed, and there are perforations by flying debris. Large holes are formed in the aluminum plates far away from the impact direction under the direct impact of the debris cloud, and the plates are almost completely destroyed.

Besides comparing the overall changes in the simulated satellite subjected to hypervelocity impact in the simulation and the test, it is also needed to further compare the differences between the debris fragment characteristic parameters in simulation results and test data. The fragment characteristic length distribution is shown in Figure 28.

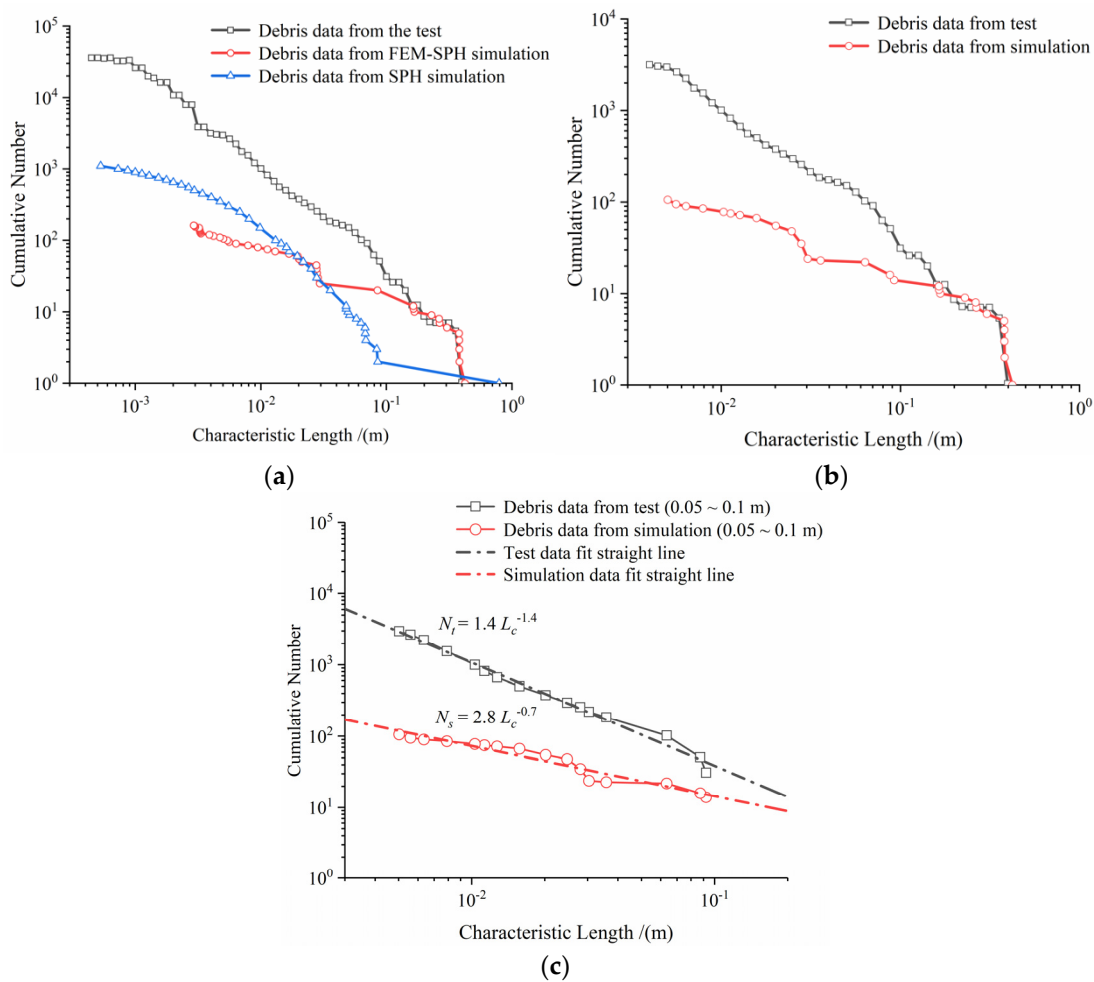


Figure 28. Comparison of fragment characteristic length distribution of the simulated satellite between simulation and test. (a) Comparison of fragment characteristic length distribution between the two simulation methods and test data; (b) comparison of characteristic length distribution between results of the finite element method-smooth particle hydrodynamics method and test data; (c) comparison of fitting lines between results of the finite element method-smooth particle hydrodynamics method and test data.

According to Figure 28, although the number of fragments obtained by the SPH method is more than that by the adaptive coupling method, it is not consistent with the test result. The fragment characteristic length calculated by the FEM-SPH adaptive coupling method exceeds 100 mm, i.e., the distribution of larger fragments is consistent with the test

data. Through Element search, it is found that the fragments with accurate characteristic length distribution are mainly large-scale debris formed after the damage of the main structural plate, central cylinder, and inner diaphragm. The consistency of these data also confirms that the adaptive coupling method produces more accurate results for the simulation of the breakup and macro damage of large-scale complex spacecraft structures subjected to hypervelocity impacts. However, from Figure 27b, there is a certain gap between the characteristic length distribution of small-size (<100 mm) fragments calculated by the FEM-SPH method and the test results. From the fitting line in Figure 27c, it can be seen that the characteristic size distribution of the simulation and the test can be fitted into a similar power function and converted based on the mathematical relationship. The characteristic length distribution functions fitted by the test and the simulation are shown in Equations (25) and (26), and the relationship between the cumulative number of fragments in the test and the simulation data is shown in Equation (27).

$$N_t = 1.4L_c^{-1.4} \tag{25}$$

$$N_s = 2.8L_c^{-0.7} \tag{26}$$

$$N_t = 0.5L_c^{-0.7} \cdot N_s \tag{27}$$

where N is the cumulative number of fragments, whose size is greater than or equal to a certain characteristic size, L_c is the number of fragments, the subscript t represents the test data, and s represents the simulation data.

Secondly, the fragment mass distribution is shown in Figure 29. As illustrated, similar to the characteristic length distribution, the statistical distribution of fragment mass data calculated by the adaptive coupling algorithm is also in the range of large masses (10~1000 g), which is consistent with the test statistics. These fragments are mainly those generated after the breakup and destruction of the main structure of the satellite. In the range of small masses (<10 g), limited by the total amount of fragments output by the simulation method, the mass distribution obtained from the simulation data is quite different compared to the test.

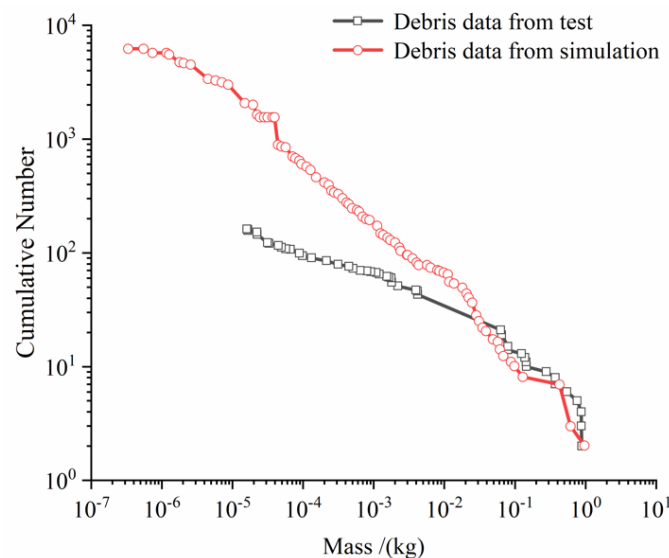


Figure 29. Comparison of fragment mass distribution of simulated satellite between simulation and test.

Finally, the relationship between fragment characteristic length and mass is shown in Figure 30. In the figure, the fragment data obtained from the characteristic length–mass simulation are highly consistent with the test data in the whole range, and Equation (28)

for the functional relationship curve of the characteristic length and mass fitted according to the simulation data and Equation (29) for the curve fitted by the test [36].

$$m_s = 10^{1.09} \cdot L_c^{2.29} \quad (28)$$

$$m_t = 10^{1.0684} \cdot L_c^{2.2591} \quad (29)$$

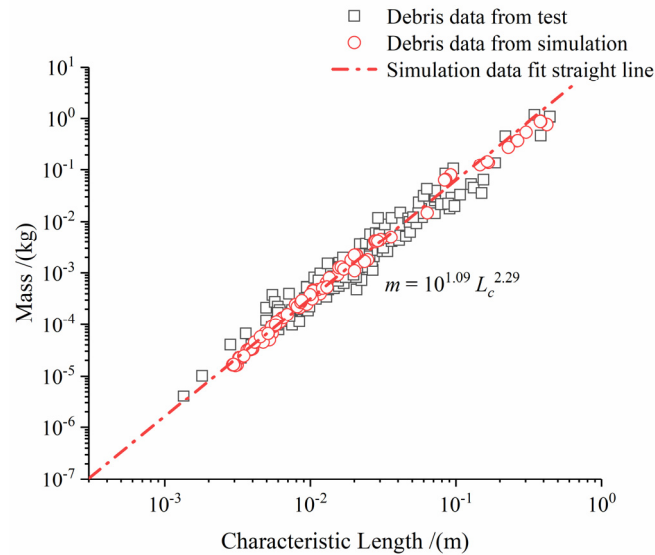


Figure 30. Comparison of fragment characteristic length–mass relationship between simulation and test.

From the coefficient and index data in the expression, it can be seen that the function curves fitted by the simulation and the test are very close. In addition, it is noted that the power exponents of the characteristic sizes in the above formula are 2.29 and 2.2591, which are different from the general three-halves power of mass and size. The reason is that the fragment characteristic size used in the debris research does not characterize the actual volume occupied by the debris fragments, but the volume of hexahedron projected by them in the three-dimensional space [36]. The actual fragment mass is less than the mass of the projected hexahedron, which shows in the functional relationship that the index of the characteristic size should be less than three. In this sense, the power exponent of the characteristic size in the above equation is also a reflection of the irregularity of fragment shape, and the coefficients $10^{1.09}$ and $10^{1.0684}$ are also parameters related to fragment material density and fragment shape. Therefore, it is deduced that the highly consistent characteristic length–mass relationship in the simulation and the test reflects that the fragment shape obtained by the FEM-SPH adaptive coupling method is generally close to the real situation.

5.4. Analysis of Simulation Results of Finite Element Method—Smooth Particle Hydrodynamics Adaptive Coupling Method

Firstly, to judge the overall breakup and damage of the satellite, through the comparison of the test photos and simulation results, it is found that using the FEM-SPH adaptive coupling method, the satellite breakup and damage are in line with the actual situation.

Secondly, the FEM-SPH adaptive coupling algorithm is suitable for the simulation of the hypervelocity impact of non-symmetric targets. In such conditions, the change of the impact position not only leads to the changes in the components and structures in the impact channel of space debris and satellites but also leads to different effects of overall damage and disintegration of the satellites. Through the same period of time after impact, the degrees of disintegration and separation between the structural plates are

obviously affected, and the target structure in and near the impact channel show more obvious mechanical responses.

Thirdly, in calculating the debris fragment characteristic parameters, through the comparative analysis of the debris characteristic length distribution, mass distribution, and characteristic length–mass relationship obtained from the simulation and the test, it is found that there is a certain gap between the debris characteristic parameters obtained by the two methods and the test data. However, the characteristic length distribution and mass distribution of the fragments with sizes greater than 100 mm obtained by the FEM-SPH method are in good agreement with the test results. Therefore, the FEM-SPH method can better simulate the macro breakup and fragmentation of models of large-scale complex structures under hypervelocity impact, and can accurately output the characteristic parameters of large-scale fragments (50 times the mesh size). In addition, it is also found that although the output of fragment characteristic parameters in the scale of 0.0001~0.1 m does not conform to the test law due to the insufficient total amount of output fragments under certain mesh accuracy, there is a unified mathematical relationship between the lines fitted by the simulation and test data, which can be derived from each other.

Finally, as for the relationship between the fragment mass and characteristic length, it is found that the fragments at all scales simulated by the FEM-SPH method conform to the characteristic length–mass relationship obtained by the test. The power exponent and coefficient of the characteristic size is, to some extent, a reflection of fragment shape. Therefore, the fragment shape simulated by the FEM-SPH adaptive coupling method is generally consistent with the actual situation, and follow-up research can be done on the fragments' aerodynamic, atmospheric reentry, or secondary damage analysis.

6. Discussion

This study aims to find appropriate numerical simulation means to address the problem of hypervelocity impact more accurately on large-scale complex spacecraft structures, so that the spacecraft's breakup, debris cloud characteristic parameters, and debris fragment distribution can be accurately simulated and analyzed, and test verification performed. When the appropriate simulation method is determined, it can be extended to the problem of hypervelocity impact on larger-scale spacecraft, space stations, and incoming missile targets, which will better guide the follow-up tests, reduce research costs, and improve research efficiency.

6.1. Analysis on the Application of Constraint Algorithm in Hypervelocity Impact Field

In the study of hypervelocity impact on spacecraft, the first essential factor is the debris cloud. Since the debris cloud and secondary debris are also important damage sources for non-monolayer targets with complex structures, the simulation algorithm needs to accurately present the profile of debris clouds and related characteristic parameters, so that researchers can conduct better follow-up observation. The second is the acquisition of the characteristic parameters of large-scale debris fragments. The characteristic length, mass, and velocity of such debris fragments may become the input for the subsequent atmospheric reentry and impact point research. The third is the small-scale debris fragments generated after impact. They may later become space debris posing potential threats to other spacecraft.

Therefore, in the study of algorithms for hypervelocity impact on spacecraft, in order to display the debris cloud, the algorithm should not delete too many elements and maintain the conservation of mass and energy. The algorithm is critical for finite element meshes and particles, mesh and particle transformation conditions, and criteria for binding constraint establishment or interaction between elements. Moreover, in the simulation of the acquisition of large-scale spacecraft fragments, it has been found that the adaptive finite element and particle coupling method can accurately calculate the structural fragments. Finally, with regard to the potentially hazardous small-size fragments, through the adaptive coupling method with a certain initial mesh fineness, a certain number of space fragments

with more real shapes can be obtained. If one wants to obtain small fragments whose number is similar to that of the real situation, in the simulation algorithm, the mesh-particle transformation conditions or the basic simulation method needs to be adjusted.

6.2. Discussion on the Influence of Mesh and Particle Size on Hypervelocity Problem

The hypervelocity impact problem is extended from the millimeter level to the centimeter or even meter level, and from the simple single-layer plate to complex spacecraft structures. If numerical simulations are used for the relevant research, the sensitivity of the algorithm to elements and particles becomes very important. For the algorithms involved in the research, regarding the calculation results of the debris cloud, it is found that the simulation method of establishing inter-node constraints to reduce element deletion represented by node separation, the formation of debris clouds is greatly affected by the mesh size. The FEM-SPG fixed coupling method, under the setting in the study, the mechanism of particle interaction is not suitable for the analysis of hypervelocity impact, and the debris cloud contour is different from the conventional situation. Both the FEM-SPH adaptive coupling and the SPH methods can obtain a better shape of debris clouds, and their characteristic parameters of the FEM-SPH adaptive coupling method are less affected by the mesh size.

As for the calculation results of debris fragment characteristics, if the full-scale study on hypervelocity impact is extended to the statistical analysis of breakup equations of different spacecraft and even missile interception, there are high requirements for the authenticity of the number of fragment output of the algorithm. It is found that both the FEM-SPH and SPH methods can output the information of fragment characteristic parameters, and the output by the adaptive coupling method is more accurate than test data. However, although the FEM-SPH method can produce fragments with clear and accurate shapes, the total amount of output fragments is greatly affected by the initial mesh size. Due to the use of the Johnson–Cook and maximum tensile stress failure models, the meshes at the crack position must be dense enough in the definition; otherwise, a large number of element failures will greatly impact the statistical results of the FEM fragments.

7. Conclusions

To address the problems in the calculation differences of the breakup, characteristic parameters of debris clouds, and fragments by various numerical simulation methods for hypervelocity impact on the full-scale model, we carried out this study. Firstly, the simulation results of the smooth particle hydrodynamics method, finite element method-smooth particle hydrodynamics adaptive coupling method, the finite element method-smoothed particle Galerkin fixed coupling method, and the node separation method under different mesh/particle sizes were compared against the test of aluminum projectile impact on the aluminum plate. It was found that the finite element method-smooth particle hydrodynamics adaptive coupling method has the advantage of low mesh sensitivity in the simulation of debris cloud characteristic parameters. Then, the accuracies of these four different numerical simulation algorithms are compared and analyzed from the perspectives of mesh sensitivity, the difference between the numerical simulation results and the exact solutions, the difference between the numerical simulation results and experimental data, and the accumulated error analysis. Therefore, the finite element method-smooth particle hydrodynamics adaptive coupling method is more suitable for the numerical simulation of large-scale hypervelocity kinetic energy impact.

Then this method was applied to the simulation and calculation of hypervelocity space debris impact on satellites. First, the suitability of this algorithm for hypervelocity impact numerical simulation of large-scale non-symmetric complex spacecraft is verified. Secondly, the fragment statistical program further developed in the study was employed and the result elements and node data were input to obtain the statistical law of fragment characteristic parameters. Comparing the statistical results of simulation data with the test results, we found that this algorithm had high accuracy in judging the overall macro breakup and damage and that the characteristic parameters and quantity distribution

were more accurate in the output of large fragments. In addition, the characteristic length–mass relationship in the full-scale range of debris output from the simulation was in good agreement with the test results. In general, although the number of fragments output by the finite element method–smooth particle hydrodynamics adaptive coupling method was less than the real situation, the authenticity of the shape and other characteristics of the output fragments was high, which is suitable for the hypervelocity impact simulation analysis of complex structures under certain requirements.

The results of this study offer different numerical algorithms for selection and show the direction for improvements in the modeling of the breakup of full-scale complex spacecraft structures and other targets subjected to hypervelocity impacts. This is a follow-up study on spacecraft hypervelocity impact: the factors influencing spacecraft breakup (multi-material, impact position, relative impact velocity, impact dip, etc.), the formula of spacecraft damage critical velocity, the engineering algorithm of spacecraft perforation diameter (multi-layer target boards) and crater depth, and the summary of spacecraft breakup model, laying a good foundation for the methods selection and establishment of numerical simulation. However, further research is needed on the limitation of the node separation algorithm to the mesh scale and the optimization of the finite element method–smooth particle hydrodynamics coupling method. The following research needs to consider the computational efficiency and the limitation of the maximum allowable error and maintain a small mesh scale, meanwhile ensuring a certain number of simulation debris output. One method is to increase the mesh density of the target damage volume and reduce the mesh density of the region less affected by impacts, so as to achieve a balance between obtaining the finite element fragment number and computational efficiency. However, using this method, it is necessary to predict the damage volume accurately through an empirical formula for specific impact conditions, which needs further study. Or improvements can be made in the material failure model and algorithm, such as integrating the mechanism of node separation and “bond” failure of the smoothed particle Galerkin method into the finite element method–smooth particle hydrodynamics adaptive coupling method, and reducing the amount of mesh-transformed particles and the demand for mesh fineness.

Author Contributions: Conceptualization, F.A.; data curation, Y.Z., F.A. and Y.L.; formal analysis, Y.Z.; investigation, Y.Z.; methodology, Y.Z. and F.A.; project administration, F.A. and C.W.; resources, F.A.; software, Y.Z. and S.L.; supervision, F.A., C.W. and J.L.; validation, F.A., C.W. and J.L.; visualization, Y.Z.; writing—original draft, Y.Z.; writing—review and editing, F.A. All authors have read and agreed to the published version of the manuscript.

Funding: This research received no external funding.

Data Availability Statement: The data used to support the findings of this study are included within the article.

Acknowledgments: All the authors would like to express our sincere gratitude to the reviewers who provided insight and expertise that greatly assisted us in revising the manuscript.

Conflicts of Interest: The authors declare no conflict of interest.

Abbreviations

HVI	Hypervelocity impact
SPH	Smooth particle hydrodynamics
FEM	Finite element method
SPG	Smoothed particle Galerkin
ALE	Arbitrary Lagrangian–Eulerian
BFS	Breadth first search
FER	Finite element reconstruction
LSTC	Livermore Software Technology Corporation

EoS	Equation of state
JC	Johnson–Cook
L_c	Fragment characteristic length
N	Cumulative number of fragments

References

- Adushkin, V.; Aksenov, O.Y.; Veniaminov, S.; Kozlov, S.; Tyurenkova, V. The small orbital debris population and its impact on space activities and ecological safety. *Acta Astronaut.* **2020**, *176*, 591–597. [[CrossRef](#)]
- Yue, L.; Yan, J.; Zhong, Q.H. Analysis of hypervelocity impact simulation algorithm. *J. Syst. Simul.* **2004**, *16*, 1941–1943.
- Smirnov, N.; Kiselev, A.; Zakharov, P. Numerical simulation of the hypervelocity impact of the ball and the spherical containment in three-material statement. *Acta Astronaut.* **2020**, *171*, 215–224. [[CrossRef](#)]
- Hockney, R.W.; Eastwood, J.W. *Computer Simulation Using Particles*, 1st ed.; CRC Press: Boca Raton, FL, USA, 1988.
- Benz, W. Smooth particle hydrodynamics: A review. In *The Numerical Modelling of Nonlinear Stellar Pulsations*; Springer: Berlin/Heidelberg, Germany, 1990; pp. 269–288.
- Benz, W.; Asphaug, E. Impact simulations with fracture. I. Method and tests. *Icarus* **1994**, *107*, 98–116. [[CrossRef](#)]
- Xu, J.; Tang, W.; Xu, Z. Numerical analysis of the characteristics of debris clouds produced by hypervelocity impacts using SPH method. *Chin. J. High Press Phys.* **2008**, *22*, 377–383.
- Liang, S.C.; Li, Y.; Chen, H.; Huang, J.; Liu, S. Research on the technique of identifying debris and obtaining characteristic parameters of large-scale 3D point set. *Int. J. Impact Eng.* **2013**, *56*, 27–31. [[CrossRef](#)]
- Chen, Y.; Chen, X. Research progress of improved whipple protective structure and related numerical simulation methods. *Explos. Shock Waves* **2021**, *41*, 33–59.
- Libersky, L.D.; Randles, P.W.; Carney, T.C.; Dickinson, D.L. Recent improvements in SPH modeling of hypervelocity Impact. *Int. J. Impact Eng.* **1997**, *20*, 525–532. [[CrossRef](#)]
- Sakong, J.; Woo, S.C.; Kim, T.W. Determination of impact fragments from particle analysis via smoothed particle hydrodynamics and k-means clustering. *Int. J. Impact Eng.* **2019**, *134*, 103387. [[CrossRef](#)]
- Zhang, X.; Jia, G.; Huang, H. Finite element reconstruction approach for on-orbit spacecraft breakup dynamics simulation and fragment analysis. *Adv. Space Res.* **2013**, *51*, 423–433. [[CrossRef](#)]
- Zhang, X.; Wang, R.; Liu, J.; Li, X.; Jia, G. A numerical method for the ballistic performance prediction of the sandwiched open cell aluminum foam under hypervelocity impact. *Aerosp. Sci. Technol.* **2018**, *75*, 254–260. [[CrossRef](#)]
- Becker, M.; Seidl, M.; Mehl, M.; Souli, M.h.; Legendre, J.F. Numerical and experimental investigation of SPH, SPG, and FEM for high-velocity impact applications. In Proceedings of the 12th European LS-DYNA Conference, Koblenz, Germany, 14–16 May 2019.
- He, Y.; Wu, Y.; Zhang, Q. Numerical simulation for the influence of impact angle on debris clouds distribution. *Trans. Beijing Instit. Technol.* **2007**, *27*, 851–854.
- Johnson, G.R. Linking of Lagrangian particle methods to standard finite element methods for high velocity impact computations. *Nucl. Eng. Des.* **1994**, *150*, 265–274. [[CrossRef](#)]
- Sauer, M. *Adaptive Kopplung des Netzfreen SPH-Verfahrens Mit Finiten Elementen zur Berechnung von Impaktvorgängen*; Universität der Bundeswehr München: Munich, Germany, 2000.
- Wang, J.; Wang, X.; Bian, L. Linking of smoothed particle hydrodynamics method to standard finite element method and its application in impact dynamics. *Explos. Shock Waves* **2007**, *27*, 522–528.
- Zhang, Z.; Qiang, H.; Gao, W. A new coupled SPH-FEM algorithm and its application to impact dynamics. *Explos. Shock Waves* **2011**, *31*, 243–249. [[CrossRef](#)]
- Deconinck, P.; Abdulhamid, H.; Hérelil, P.; Mespoulet, J.; Puillet, C. Experimental and numerical study of submillimeter-sized hypervelocity impacts on honeycomb sandwich structures. *Proc. Eng.* **2017**, *204*, 452–459. [[CrossRef](#)]
- He, Q.G.; Chen, X.; Chen, J.F. Finite element-smoothed particle hydrodynamics adaptive method in simulating debris cloud. *Acta Astronaut.* **2020**, *175*, 99–117. [[CrossRef](#)]
- Hu, W.; Wu, Z.T.; Wu, Y.C. Advanced simulation technology of LS-DYNA simulation connection failure and structure impact. In Proceedings of the Annual Meeting and Exhibition of the Society of Automotive Engineers of China, Shanghai, China, 22–24 October 2019; pp. 311–318.
- Zhang, X.; Chen, Y.; Jia, G.; Huang, H. Node-separation FEM simulation of typical spacecraft protective structure. *J. Astronaut* **2013**, *34*, 597–604.
- Zhang, X.; Jia, G.; Huang, H. Numerical investigation of aluminum foam shield based on fractal theory and node-separation FEM. *Chin. J. Aeronaut.* **2011**, *24*, 734–740. [[CrossRef](#)]
- Liu, T.; Zeng, Z.; Zhang, X.; Qiu, X.; Cai, J.; Li, L. Performance of polyimide film under hypervelocity impact of micro flyer: Numerical and analytical modeling. *Acta Astronaut.* **2019**, *160*, 138–146. [[CrossRef](#)]
- Rumyantsev, B.; Guk, I.; Kozachuk, A.; Mikhaylin, A.; Pavlov, S.; Silnikov, M. Interaction between hypervelocity elongated projectile and screen protection of space vehicles. *Acta Astronaut.* **2019**, *163*, 73–78. [[CrossRef](#)]
- Shakirzyanova, V.V.; Selivanov, V.V.; Silnikov, M.V.; Malishchuk, T.S. Behavior of multilayer transparent spacecraft elements during high-speed impact with compact impactors. *Acta Astronaut.* **2021**, *180*, 119–124. [[CrossRef](#)]

28. Toor, Z.S.; Baluch, A.H. Dynamic evaluation of aluminum alloys using a virtual framework. *Acta Astronaut.* **2021**, *189*, 567–575. [[CrossRef](#)]
29. Schimmerohn, M.; Matura, P.; Watson, E.; Durr, N.; Altes, A.; Cardone, T.; de Wilde, D.; Krag, H.; Schäfer, F. Numerical investigation on the standard catastrophic breakup criteria. *Acta Astronaut.* **2021**, *178*, 265–271. [[CrossRef](#)]
30. Meshkov, V.V.; Fedosov, Y.A.; Filatova, N.N. An integrated system for modeling hypervelocity interaction of solids. *Acta Astronaut.* **2021**, *178*, 606–615. [[CrossRef](#)]
31. Libersky, L.D.; Petschek, A.G.; Carney, T.C.; Hipp, J.R.; Allahdadi, F.A. High strain Lagrangian hydrodynamics: A three-dimensional SPH code for dynamic material response. *J. Comput. Phys.* **1993**, *109*, 67–75. [[CrossRef](#)]
32. Wu, C.; Koishi, M.; Hu, W. A displacement smoothing induced strain gradient stabilization for the meshfree Galerkin nodal integration method. *Comput. Mech.* **2015**, *56*, 19–37. [[CrossRef](#)]
33. Wu, C.; Wu, Y.; Crawford, J.E.; Magallanes, J.M. Three-dimensional concrete impact and penetration simulations using the smoothed particle Galerkin method. *Int. J. Impact Eng.* **2017**, *106*, 1–17. [[CrossRef](#)]
34. Piekutowski, A.J. *Formation and Description of Debris Clouds Produced by Hypervelocity Impact*; National Aeronautics and Space Administration: Huntsville, AL, USA, 1996; 272p.
35. Piekutowski, A.J. Characteristics of debris clouds produced by hypervelocity impact of aluminum spheres with thin aluminum plates. *Int. J. Impact Eng.* **1993**, *14*, 573–586. [[CrossRef](#)]
36. Liu, S.; Lan, S.; Ma, Z.; Li, Y.; Huang, J. Experimental study on the characteristics of satellite hypervelocity impact fragments. *J. Astronaut.* **2012**, *33*, 1347–1353.
37. Veldman, R.; Ari-Gur, J.; Clum, C.; DeYoung, A.; Folkert, J. Effects of pre-pressurization on blast response of clamped aluminum plates. *Int. J. Impact Eng.* **2006**, *32*, 1678–1695. [[CrossRef](#)]
38. Vahedi, K.; Khazraian, N. Numerical modeling of ballistic penetration of long rods into ceramic/metal armors. In Proceedings of the 8th International LS-DYNA Users Conference, Dearbon, MI, USA, 19–21 May 2004; pp. 39–50.
39. Varas, D.; Zaera, R.; López-Puente, J. Numerical modelling of the hydrodynamic ram phenomenon. *Int. J. Impact Eng.* **2009**, *36*, 363–374. [[CrossRef](#)]
40. Bless, S. Bumper debris cloud structure estimated by shock calculations. *J. Phys. IV* **1991**, *1*, 903–908. [[CrossRef](#)]
41. Piekutowski, A.J. A simple dynamic model for the formation of debris clouds. *Int. J. Impact Eng.* **1990**, *10*, 453–471. [[CrossRef](#)]
42. De Chant, L.J. An explanation for the minimal effect of body curvature on hypervelocity penetration hole formation. *Int. J. Solids Struct.* **2004**, *41*, 4163–4177. [[CrossRef](#)]
43. Smirnov, N.; Betelin, V.; Nikitin, V.; Stamov, L.; Altoukhov, D. Accumulation of errors in numerical simulations of chemically reacting gas dynamics. *Acta Astronaut.* **2015**, *117*, 338–355. [[CrossRef](#)]
44. Smirnov, N.; Betelin, V.; Shagaliev, R.; Nikitin, V.; Belyakov, I.; Deryuguin, Y.N.; Aksenov, S.; Korchazhkin, D. Hydrogen fuel rocket engines simulation using LOGOS code. *Int. J. Hydrogen Energy* **2014**, *39*, 10748–10756. [[CrossRef](#)]